

SIMULATION ON INTERFEROMETRIC FIBER OPTIC GYROSCOPE
WITH AMPLIFIED OPTICAL FEEDBACK

A THESIS SUBMITTED TO
THE GRADUATE SCHOOL OF NATURAL AND APPLIED SCIENCES
OF
THE MIDDLE EAST TECHNICAL UNIVERSITY

BY

BAŞAK SEÇMEN

IN PARTIAL FULLFILMENT OF THE REQUIREMENTS FOR THE DEGREE
OF
MASTER OF SCIENCE
IN
THE DEPARTMENT OF PHYSICS

SEPTEMBER 2003

ABSTRACT

SIMULATION ON INTERFEROMETRIC FIBER OPTIC GYROSCOPE WITH AMPLIFIED OPTICAL FEEDBACK

Seçmen, Başak

M.S., Department of Physics

Supervisor: Assoc. Prof. Dr. Serhat Çakır

September 2003, 87 Pages

Position and navigation of vehicle in two and three dimensions have been important as being advanced technology. Therefore, some system has been evaluated to get information of vehicle's position. Main problem in navigation is how to determine position and rotation in three dimensions. If position and rotation is determined, navigation will also be determined with respect to their initial point. There is a technology that vehicle velocity can be discovered, but a technology that rotation can be discovered is needed. Sensor which sense rotation is called gyroscope. If this instrument consists of optical and solid state material, it's defined by Fiber Optic Gyroscope (FOG).

There are various studies in order to increase the sensitivity of fiber optic gyroscopes, which is an excellent vehicle for sensing rotation. One of them is interferometric fiber optic gyroscope with amplified optical feedback (FE_FOG). In this system, a feedback loop, which sent the output pulse through the input again, is used. The total output is the summation of each interference and it is in pulse state. The peak position of the output pulse is shifted when rotation occurs. Analyzing this shift, the rotation angle can be determined.

In this study, fiber optic gyroscopes, their components and performance characteristics were reviewed. The simulation code was developed by VPIsystems and I used VPItransmissionMakerTM software in this work. The results getting from both rotation and nonrotation cases were analyzed to determine the rotation angle and sensitivity of the gyroscope.

Key words: Fiber optic gyroscope, Sagnac interferometer, EDFA, Amplified feedback loop, simulation.

ÖZ

YÜKSELTİLMİŞ OPTİKSEL GERİ BESLEME DÖNGÜLÜ İNERFEROMETRİK FİBER OPTİK JİROSKOP SİMÜLASYONU

Seçmen, Başak

Master, Fizik Bölümü

Tez Yöneticisi: Doç. Dr. Serhat Çakır

Eylül 2003, 87 Sayfa

Gelişen teknolojiye paralel olarak araçların veya cisimlerin iki ve üç boyutlu uzayda konum ve pozisyonunun bilinmesi önem kazanmıştır. Bu yüzden, bu pozisyonlamanın yapılabilmesi için çeşitli sistemler geliştirilmiştir. Yer tayinindeki en temel problem, üç boyutlu uzayda pozisyon ve açısal dönmenin nasıl ölçüleceğidir. Eğer bu nicelikleri belirleyebilirsek, bilinen bir başlangıç noktasına göre aracın hareket vektörünü ve konumunu hesaplayabiliriz. Aracın hız vektörünü belirleyebilecek teknoloji mevcuttur, fakat dönmeyi algılayacak teknolojiye ihtiyaç duyulmaktadır. Dönmeyi algılayan sensörlere jiroskop denir. Sagnac İnterferometrenin keşfi ve yarı iletken teknolojisinin gelişmesiyle, jiroskoplar tamamen optiksel ve yarı iletken materyallerden oluşan bir cihaza dönüşmüştür. Bu cihaza Fiber Optik Jiroskop (FOG) denmektedir.

Açısal dönmeyi ölçmek için mükemmel bir cihaz olan fiber optik jiroskopun duyarlılığını artırmak için çeşitli çalışmalar yapılmaktadır. Bunlardan biri de yükseltilmiş geri bildirim döngülü interferometrik fiber optik jiroskoptur. Bu sistemin çalışması jiroskoptan alınan çıktının tekrar girişten gönderilmesini sağlayan bir döngü oluşturularak darbeler elde etme esasına dayanmaktadır. Jiroskobun dönme açısına bağlı olarak sapma gösteren bu darbeler incelenerek dönme miktarı belirlenir.

Bu çalışmada fiber optik jiroskopların özellikleri incelendi. VPIsystems tarafından geliştirilen VPItransmissionMaker™ yazılımı kullanılarak yükseltilmiş geri bildirim döngülü interferometrik fiber optik jiroskop simülasyonu yapıldı. Jiroskobun hareketsiz konumunda ve çeşitli açılarda dönmesi durumlarında elde edilen sonuçlar karşılaştırılarak dönme açısı tayini yapıldı ve duyarlılığı incelendi.

Anahtar kelimeler: Fiber optik jiroskop, Sagnac interferometre, EDFA, Yükseltilmiş geri besleme döngüsü, simülasyon.

ACKNOWLEDGMENTS

I would like to acknowledge gratefully to my supervisor Assoc. Prof. Dr. Serhat akır for his guidance, support and encouragements during this thesis. I would also like to thank to Dr. Ali Alaakır for his suggestions and comments. I am also grateful to my friends, Bařak Ballı and F. Feza Bykřahin for their helps and suggestions. Finally, I wish to thank my family for their supports and encouragements.

TABLE OF CONTENTS

ABSTRACT.....	iii
ÖZ.....	v
ACKNOWLEDGEMENTS.....	vii
TABLE OF CONTENTS.....	viii
LIST OF FIGURES.....	xi
CHAPTERS	
1. OVERVIEW OF FIBER OPTIC GYROSCOPES.....	1
1.1 Introduction.....	1
1.1.1 Review of Wave Physics.....	3
1.1.2 Interference of Waves.....	5
1.2 Basic Principle of The Fiber Optic Gyroscope.....	11
1.2.1 Sagnac Effect.....	11
1.2.2 Bias Modulation.....	14
2. FOG CONSTRUCTION AND COMPONENTS.....	19
2.1 Reciprocity.....	19
2.2 Fiber Coil.....	21
2.3 Light Source.....	21
2.4 Coupler.....	23
2.5 Phase Modulators.....	24
2.6 Detector.....	26
3. GYRO PERFORMANCE.....	27
3.1 Noise.....	27
3.1.1 Shot Noise.....	27
3.1.2 Johnson Noise.....	28
3.1.3 Thermal Phase Noise.....	28
3.1.4 Relative Intensity Noise.....	28

3.2 Bias Stability.....	28
3.2.1 Bias Error Mechanisms.....	28
3.2.1.1 Modulator Error.....	28
3.2.1.1.A) Nonlinearity.....	28
3.2.1.1.B) Intensity Modulation.....	29
3.2.1.2 Secondary Waves.....	29
3.2.1.3 Nonreciprocal Effects.....	29
3.3 Input Axis Alignment.....	30
3.4 Deadzone (Lock-In).....	31
3.5 Scale Factor Stability.....	31
4. SIMULATION ON INTERFEROMETRIC FIBER	
OPTIC GYROSCOPE WITH AMPLIFIED OPTICAL	
FEEDBACK (FE-FOG).....	32
4.1 Properties of Simulation Program, VPItransmissionmaker™	32
4.2 Signal Representations.....	33
4.3 Global Variables.....	33
4.4 Interferometric Fiber Optic Gyroscope	
with Amplified Optical Feedback (FE-FOG).....	35
4.5 Configuration of A FE_FOG.....	36
4.6 Theory.....	37
4.7 Simulations And Discussions.....	40
4.8 Modules Used in the Schematic.....	42
4.8.1 LaserCW.....	42
4.8.2 X Coupler And X Coupler Bi-Directional.....	43
4.8.3 Phase Shift.....	43
4.8.4 Sine Generator (Electrical)	43
4.8.5 Multiple Output Connector (Fork)	44
4.8.6 Modulator Phase.....	44
4.8.7 Photodiode (Pin).....	44
4.8.8 Time Domain Fiber.....	45
4.8.9 Ideal Amplifier with Wavelength Independent Gain	46
4.9 Results.....	47

5. CONCLUSION.....	55
REFERENCES.....	57

APPENDICES

A. MODULES USED IN THE SIMULATION	60
A.1 LaserCW	60
A.2 X Coupler.....	64
A.3 X Coupler Bidirectional.....	66
A.4 Phase Shift.....	66
A.5 Sine Generator (Electrical).....	69
A.6 Multiple Output Connector (Fork).....	71
A.7 Modulator Phase.....	72
A.8 Photodiode Pin.....	74
A.9 Null Source.....	77
A.10 Ground.....	78
A.11 Time Domain Fiber.....	79
A.12 Ideal Amplifier with Wavelength Independent Gain.....	84

LIST OF FIGURES

1.1	Propagation of monochromatic wave.....	3
1.2	March-Zender Interferometer.....	5
1.3	Interferogram for monochromatic waves.....	7
1.4	Interferogram for polychromatic waves.....	8
1.5	Gaussian spectrum of $S(f)$ centered about f_0	9
1.6	Interference fringe of coherence function for $\tau \gg \tau_c$	10
1.7	Interference fringe of coherence function for $\tau \approx \tau_c$	10
1.8	Sagnac-ring interferometer.....	11
1.9	a) Sagnac-ring interferometer b) Simplified calculation of the Sagnac-effect.....	12
1.10	Sensitivity at various points on interferogram.....	15
1.11	Method to inject relative phase shift between CW and CCW waves.....	16
1.12	Sinusoidal bias modulation: detector signal with finite Sagnac phase shift	18

2.1	Reciprocal configuration.....	20
2.2	Reciprocal use of coupler.....	23
2.3	PZT modulator.....	25
2.4	Electro-optic modulator	25
3.1	Input axis alignment.....	30
3.2	Transfer functions for an ideal fiber gyro and for a fiber gyro with deadzone.....	31
4.1	Global parameters.....	35
4.2	Configuration of the FE_FOG.....	36
4.3	Schematic of the simulation.....	41
4.4	Parameters of Laser CW.....	42
4.5	Parameters of Sine Generator.....	43
4.6	Parameters of Photodiode PIN.....	44
4.7	Parameters of Time Domain Fiber in Sagnac Loop.....	45
4.8	Parameters of Ideal Amplifier.....	46
4.9	Output signal for $\phi_s = 0$, $\phi_e = 1,9$ rad.....	48

4.10	Later output pulses for $\phi_s = 0$, $\phi_e = 1,9$ rad.....	48
4.11	Output signal for $\phi_s = 0$, $\phi_e = 0,6$ rad.....	49
4.12	Comparison between two gain values (a) 8 dB and (b) 9.3 dB for $\phi_e = 1.24 \pi$ rad.....	49
4.13	Results for $\phi_e = 0,6$ rad.....	51
4.14	Results for $\phi_e = 1,9$ rad.....	52
4.15	Time shift of the output peak as the function of rotation rate with different phase modulation $\phi_e = 0,6$ rad, $\phi_e = 1,9$ rad.....	53
4.16	Comparison between (a) positive rotation $\phi_s = 20^\circ$ and (b) negative rotation $\phi_s = -20^\circ$, when $\phi_e = 1.24 \pi$ rad.	54
A.1	Schematic of the modeled DFB CW laser.....	62
A.2	Implementation of the XCouplerBi Galaxy.....	67
A.3	Noise equivalent diagram of a PIN-Direct-Receiver.....	76

CHAPTER 1

OVERVIEW OF FIBER OPTIC GYROSCOPES

1.1 Introduction

The second half of the 20th century is marked not only by social changes; but also intensive and thorough investigations in fundamental and applied science. Two aspects are to be of the paramount importance in the field of navigation: 1) creation of global satellite navigation systems, such as Transit, GPS and GLONASS; 2) the advent of a new generation of inertial navigation sensors -laser and fiber optical gyros (LG and FOG). These optical devices, making use of fundamental properties of electromagnetic waves, provide a basis for a new line of investigations in inertial navigation and make it possible to give up the fast rotating rotor. This situation opens a possibility to use new progressive technology in mass production.

Exceptional properties of optical gyros (high accuracy, wide dynamic range, non-sensitivity to linear acceleration, et al.) stimulated the evolution of various highly accurate strapdown inertial navigation systems (SINS). Integration of SINS based on optical, gyros with Satellite Navigation Systems, such as GPS and GLONASS, allows new positive properties necessary for dual usage in military and commercial technology. It is necessary to note considerable and extremely important progress in *FOG* in the last few years due to deeper understanding of physical processes in electromagnetic wave propagation in optical fiber and a wide use of integral optics. All this permits realization of an optimal architecture of *FOG* and using of micromechanical sensors to create a new modification of low life-cycle cost, small-sized and low production cost SINS [1].

There is tremendous application for rotation sensing in navigation, surveying, oil well drilling, and even spacecraft stabilization. A potentially huge market is in automobiles.

The advantages of a fiber gyroscope over a mechanical gyroscope are that there are no moving parts, no warm-up time is required, and there is no sensitivity to acceleration. They also promise to be low in cost.

The required accuracy for a gyroscope depends on the application. Short-flight missile and automobile applications can probably be satisfied with an accuracy or 10 degree per hour. To appreciate this term, consider that the earth rotates at 15 degree per hour, and the hour hand on a clock rotates at 30 degree per hour. Both of these are considered to be relatively large rotation rates from a gyroscope's point of view. Aircraft navigation requires an accuracy of 10^{-3} degree per hour. [2]

The basic navigation problem is how to determine position and angular orientation (“attitude”) while in 3-dimensional space. Using known initial position and attitude, current position and attitude can be calculated from measured time-dependent velocities (v) and angular velocities (Ω).

$$x(t) = x_0 + \int_0^t v_x(t) dt \quad (1.1)$$

$$\theta(t) = \theta_0 + \int_0^t \Omega_x(t) dt \quad (1.2)$$

These relations are functions of position and angular orientation. In order to measure angular velocity $\Omega(t)$, gyroscope is used.

1.1.1 Review of Wave Physics

Periodic disturbance propagating through the medium or vacuum is called wave. If the displacement of every point on string oscillates sinusoidally, it is called monochromatic wave. In other words, each point of string come the same position in a time period T . A monochromatic wave has a single, well-defined distance λ between successive wave peaks at a fixed instant in time.

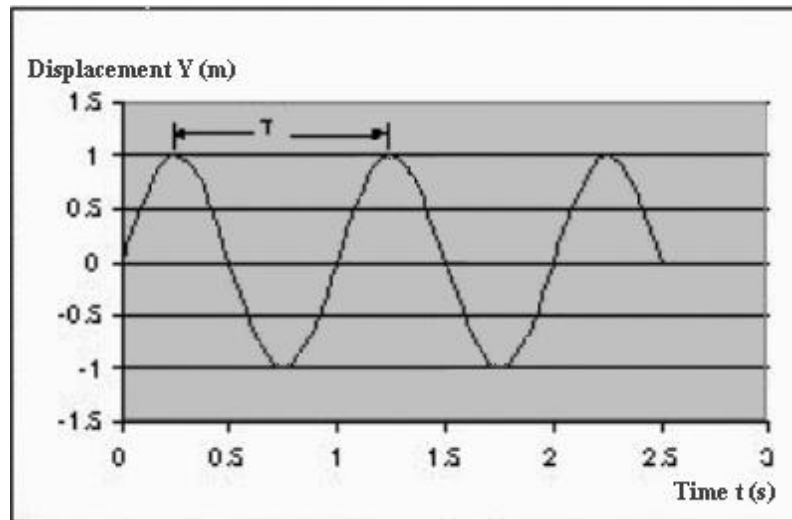


Figure 1.1. Propagation of monochromatic wave

Wave phase velocity (v_{ph}) is the speed at which successive wave peaks pass a fixed location in the medium. Relation between wavelength, frequency and phase velocity is $v_{phase} = \lambda * f$. Fundamental wave propagation equation is defined as

$$\frac{\partial^2 y(x,t)}{\partial x^2} = \frac{1}{v_{ph}^2} \frac{\partial^2 y(x,t)}{\partial t^2}. \quad (1.3)$$

The general solutions to wave equation is $y(x,t) = F(x \pm v_{phase} t)$ where $F()$ is any arbitrary function [3].

Light wave is an electromagnetic wave. Electric (\vec{E}) and magnetic (\vec{B}) fields oscillate simultaneously. Light waves can propagate in a vacuum or in media. Electric field is plotted to represent wave oscillations.

Maxwell's equations for electric and magnetic fields in vacuum;

$$\nabla \cdot \vec{E} = 0 \quad \nabla \cdot \vec{B} = 0 \quad (1.4)$$

$$\nabla \times \vec{E} = -\frac{\partial \vec{B}}{\partial t} \quad \nabla \times \vec{B} = \mu_0 \epsilon_0 \frac{\partial \vec{E}}{\partial t} \quad (1.5)$$

Wave equations are obtained from curl ($\nabla \times$) of equations (1.5) using identity $\nabla \times \nabla \times E = \nabla(\nabla \cdot E) - \nabla^2 E$.

$$\nabla^2 E = \mu_0 \epsilon_0 \frac{\partial^2 E}{\partial t^2} \quad (1.6)$$

$$\nabla^2 B = \mu_0 \epsilon_0 \frac{\partial^2 B}{\partial t^2} \quad (1.7)$$

Here μ_0 is permeability of vacuum and ϵ_0 is permittivity of vacuum. In fiber optic gyroscopes light wave does not propagate through vacuum but propagates through fused silica fiber. There are two important differences from vacuum case:

→ Maxwell equations contain terms for finite charge and current density.

→ Fiber permittivity is $\epsilon = \frac{\epsilon_0}{n}$ and permeability is $\mu = \frac{\mu_0}{n}$ where n is the fiber

refractive index.

General solution to wave equation is

$$E(x,t) = E_0 \sin(kx - \omega t) \hat{y}, \text{ where } k = 2\pi / \lambda, \omega = 2\pi f. \quad (1.8)$$

Wave accelerates any nearby charge in the y -direction; power is deposited into charge y -degree of freedom. This wave is said to be *polarized* along y .

Wave carries energy. Power carried by wave across unit area is;

$$P(x,t) = c \epsilon_0 |E(x,t)|^2 = c \epsilon_0 E_0^2 \sin^2(kx - \omega t) \quad (1.9)$$

If the wave is y -polarized then power deposited along y -direction. If the wave is x - and y -polarized then power has E_x and E_y components. ($P \propto E_x^2 + E_y^2$)

Time-averaged power over one wave cycle is

$$\langle P(x,t) \rangle = c\epsilon_0 E_0^2 \langle \sin^2(kx - \omega t) \rangle = \frac{c\epsilon_0 E_0^2}{2}. \quad (1.10)$$

For a single monochromatic wave, time-averaged power is independent of time and position. [4]

$$\langle P \rangle = P_0 = c\epsilon_0 E_0^2 / 2 \quad (1.11)$$

1.1.2 Interference of Waves

Interferometer is a device, which splits light waves into two components, which travel different paths and recombine after some relative propagation phase delay $\Delta\phi$. There are a lot of kinds of interferometer. One of them is March-Zender interferometer.

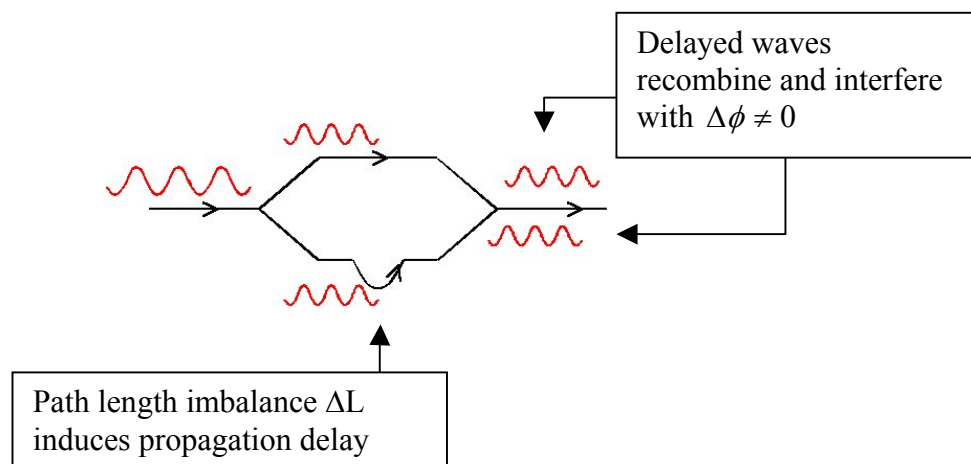


Figure 1.2. March-Zender Interferometer

If input wave is

$$\vec{E}_{in} = E_0 \hat{y} \sin(kx - wt), \quad (1.12)$$

then split waves are

$$\vec{E}_1(x, t) = E_1 \hat{y} \sin(kx - wt) \text{ and} \quad (1.13)$$

$$\vec{E}_2(x, t) = E_2 \hat{y} \sin(kx - wt + \Delta\phi), \text{ where } E_1^2 + E_2^2 = E_0^2. \quad (1.14)$$

When these waves recombine, wave equation becomes;

$$\vec{E}_{out}(x, t) = \hat{y} [E_1 \sin(kx - wt) + E_2 \sin(kx - wt + \Delta\phi)]. \quad (1.15)$$

According to $\langle P(x, t) \rangle = c\epsilon_0 \langle |E(x, t)|^2 \rangle$, time-averaged power of output wave can be computed as;

$$\begin{aligned} \langle P(x, t) \rangle &= c\epsilon_0 \left[\frac{E_1^2}{2} + \frac{E_2^2}{2} + \langle 2E_1E_2 \sin(kx - wt) \sin(kx - wt + \phi) \rangle \right] \\ &= c\epsilon_0 \left[\frac{E_1^2}{2} + \frac{E_2^2}{2} + E_1E_2 \langle \cos(\phi) - \cos(2kx - 2wt + \phi) \rangle \right] \\ &= P_1 + P_2 + 2\sqrt{P_1P_2} \cos\phi \end{aligned} \quad (1.16)$$

If $P_1 = P_2 = P$ (%50-%50 power split) then

$$\langle P \rangle = 2P(1 + \cos\Delta\phi) = \frac{I_0}{2}(1 + \cos\Delta\phi) \quad (1.17)$$

where I_0 is detector power when $\Delta\phi = 0$.

Plot of detector power vs. phase shift is called “Interferogram”.

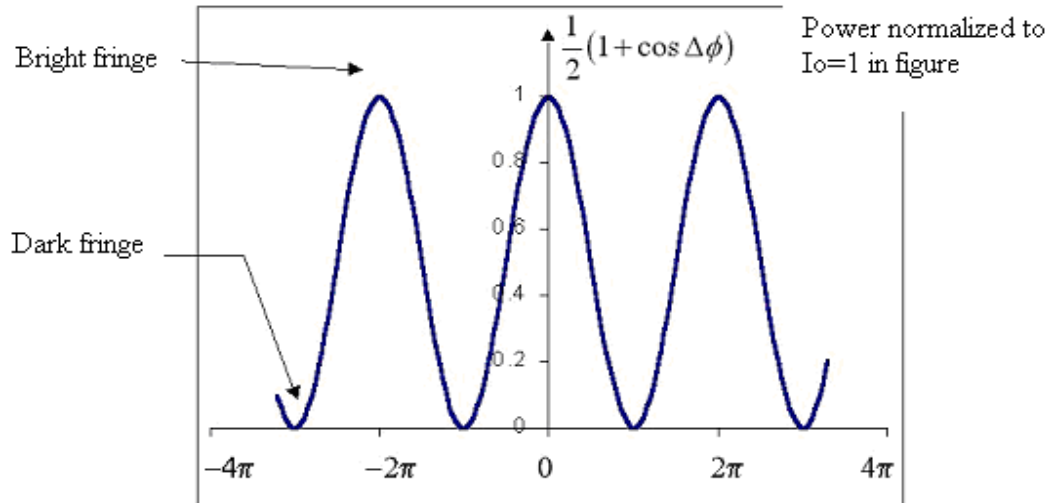


Figure 1.3. Interferogram for monochromatic waves

When monochromatic waves of identical wavelength interfere, the interferogram is periodic with period $\Delta\phi = 2\pi$ over the entire domain $\Delta\phi = [-\infty, \infty]$. These waves are said to interfere “coherently”. [5]

Consider light source containing many wavelengths λ_i . If this light passes through March-Zender interferometer of path imbalance ΔL , relative phase shift between waves of length λ_i is $\Delta\phi(\lambda_i) = 2\pi\Delta L/\lambda_i$.

Bright and dark fringes from various wavelengths overlap, ‘smearing’ the interferogram; a smeared interferogram is the interference of light with “finite coherence”.

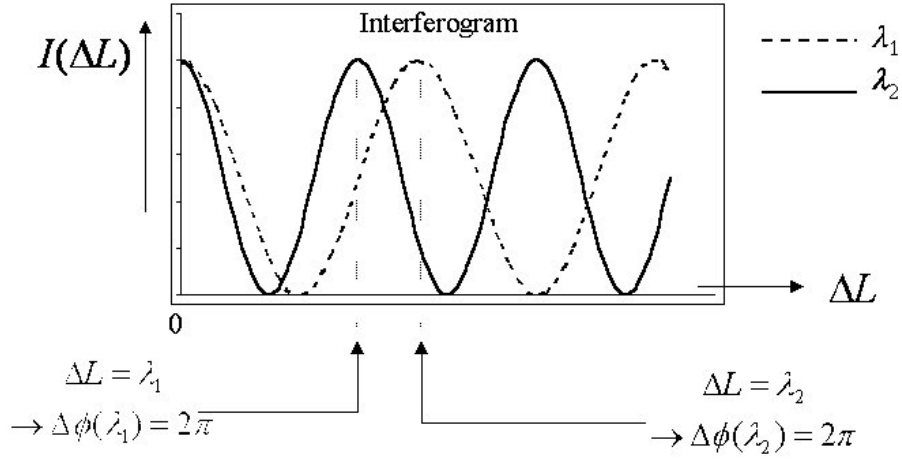


Figure 1.4. Interferogram for polychromatic waves

Electrical field amplitude $E(t)$ is time-dependent for light source of finite spectral width because the various light frequencies (wavelengths) beat together. If we describe $E(t)$ with Fourier components (frequency space convenient)

$$a(f) = \int_{-\infty}^{\infty} E(t) e^{-2\pi f t} dt \quad \text{and} \quad E(t) = \int_{-\infty}^{\infty} a(f) e^{2\pi f t} df \quad (1.18)$$

When the source spectrum passes through MZ interferometer, there occurs a relative time delay $\tau = c/\Delta L$ between recombining waves. The wave coming from path 1 is $\frac{1}{2}E(t)$ while the other wave coming from path 2 is $\frac{1}{2}E(t + \tau)$.

Time averaged output power is $\langle P \rangle = \frac{I_0}{4} \langle E(t) + E(t - \tau) \rangle$.

In this case, there is no single, well-defined period. Thus the time averaging must be taken over all time.

$$\langle E(t) \cdot E^*(t - \tau) \rangle = \lim_{T \rightarrow \infty} \frac{1}{T} \int_{-T}^T E(t) \cdot E^*(t - \tau) dt \quad (1.19)$$

The integral is the familiar autocorrelation function of $C(\tau)$;

$$C(\tau) = \langle E(t) \cdot E^*(t - \tau) \rangle.$$

Now the Wiener-Khintchine theorem relates the electric field autocorrelation function $C(\tau)$ and power spectrum $S(f)$;

$$S(f) = \int_{-\infty}^{\infty} C(\tau) e^{-2\pi i f \tau} d\tau \quad \text{and} \quad C(\tau) = \int_{-\infty}^{\infty} S(f) e^{2\pi i f \tau} df \quad (1.20)$$

Often the source spectrum is centered about a mean frequency f_0 (like Gaussian spectrum). ‘Centered’ spectrum is defined as $S_c(f) = S(f' + f_0)$.

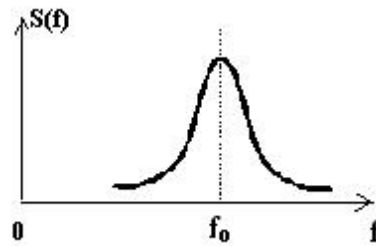


Figure 1.5. Gaussian spectrum of $S(f)$ centered about f_0

Considering Fourier transform and symmetry of Gaussian and Lorentzian spectra, using the relation $C_c(0) = \langle |E(t)|^2 \rangle$, we finally get

$$\langle P \rangle = \frac{I_0}{2} [1 \cos(2\pi f_0 \tau) \Gamma(\tau)] \quad \text{where } \tau = 0. \quad (1.21)$$

Here we have introduced the coherence function $\Gamma(\tau)$ defined as the normalized, centered autocorrelation function. The coherence time (width) is usually defined as

$$\tau_c = \int_{-\infty}^{\infty} |\Gamma(\tau)|^2 dt.$$

For $\tau \gg \tau_c$ the interference fringes vanish.

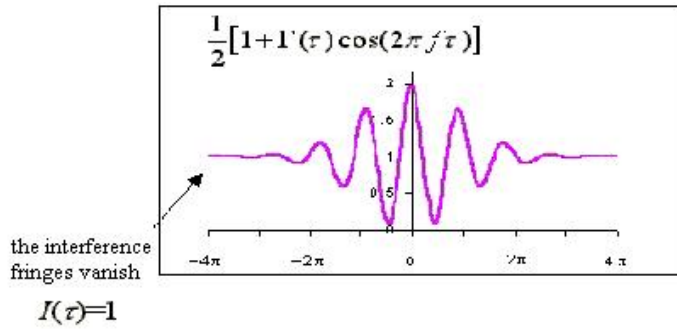


Figure 1.6. Interference fringe of coherence function for $\tau \gg \tau_c$

As τ_c increases, the fringe visibility remains high for larger delays τ .

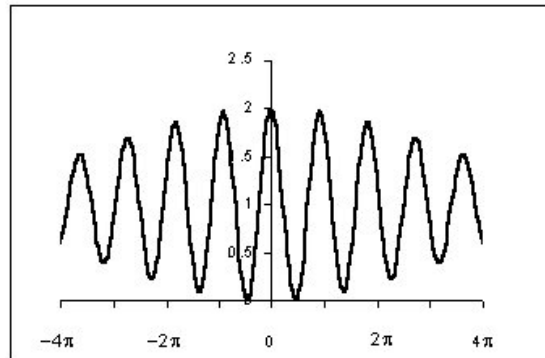


Figure 1.7. Interference fringe of coherence function for $\tau \approx \tau_c$

As $\tau_c \rightarrow \infty$, the situation approaches that of monochromatic waves: fringe visibility persists for infinite τ .

Now we can interpret all these calculations and descriptions. If an optical wave train is split and one component is time delayed relative to the other, the coherence time τ_c is the maximum time delay, which still yields a visible interferogram after recombining the two beams. The coherence length ($L_c = c \cdot \tau_c$) is roughly the maximum path length imbalance through which the split waves can pass and still yield a visible interferogram after recombination [6].

1.2 Basic Principle of the Fiber Optic Gyroscope

1.2.1 Sagnac Effect

An "observer" inside a rotating system has the task to get information about the absolute rotation of his system without getting in touch with the outer world and without using a mechanical gyro. In a first attempt he might think to measure centrifugal forces which act on a test specimen with the mass m . If he has additional knowledge about the distance r between his position and the center of rotation it should be easy to calculate the rotation rate Ω by using the expression:

$$F_{centrifugal} = m \cdot r \cdot \Omega^2. \quad (1.22)$$

But if the value of r is not known, -and generally that's the case -our "observer" has a problem: he can try to find this point inside the rotating system where the rotation dependent force will vanish, - that's the center of rotation, -but if this point is not inside of his system he will fail. A solution of this problem could be a "traveling time experiment", which enables the "observer" inside the rotating box to measure the traveling time of a signal, which propagates around a closed loop. The result of this experiment depends on the geometrical properties of the loop (circumference L or loop area A), on the signal velocity and on the rotation rate Ω of the entire system. This is the core of the Sagnac effect.

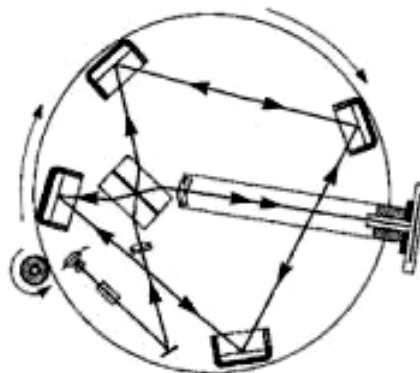


Figure 1.8. Sagnac-ring interferometer

In a second step this experiment can be improved by measuring the traveling time difference of two counter propagating signals which use the same loop. The advantage is tremendous:

- the sensitivity against the rotation rate is doubled;
- the output is now independent from the signal velocity.

This is the way how the Sagnac effect is actually used.

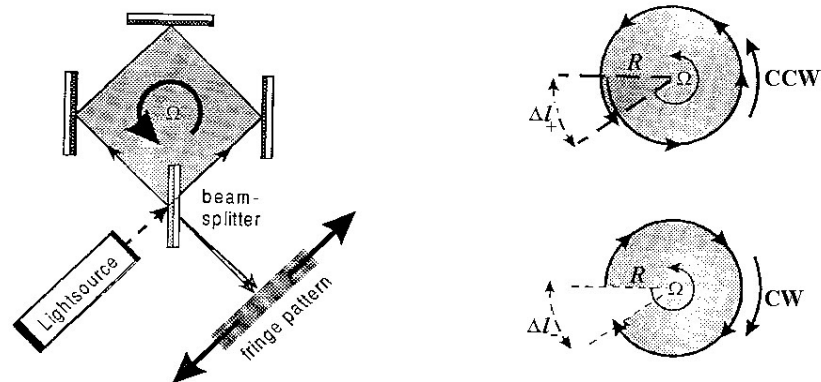


Figure 1.9. a) Sagnac-ring interferometer b) simplified calculation of the Sagnac-effect

Figure 1.9-a shows the basic elements of a ring interferometer. Two wavetrains, created by a beamsplitter, are traveling around the ring interferometer in opposite directions. If the beams are combined (superposed) after one circle they form an interference fringe pattern, which is made visible on a screen or registered by means of a photodetector.

The light source, the beam guiding system (mirrors, prisms or glass fiber), combining optics, screen and/or photodetector, -all these elements are mounted on a platform. If the whole system rotates around an axis perpendicular to the plane of the counter propagating wavetrains, the fringe pattern will be shifted proportional to the rotation rate.

The actual effect is based on a traveling time -, or phase-difference between the two wavetrains. This leads to a shift of the interference fringe pattern, and this again can easily be detected [7].

A very simple calculation of the magnitude of this effect is based on circular beam guiding configuration (Fig 2.2-b). The following parameters are used;

R	Radius of the beam guiding system
$L=2\pi.R$	Circumference of the beam guiding system
$A=\pi.R^2$	Area of the beam guiding system
c	light -/signal velocity
$\delta t=L/c = 2\pi R/c$	Traveling time of the wavetrains for one circle
Ω	rotation rate of the beam guiding system

Light enters and exits the loop at a point fixed on the fiber. If the coil rotates, the entry/ exit point rotates with fiber. There occurs a time difference for counter propagating light waves to complete one loop.

$$t_{CW} = \frac{R(2\pi - \Omega t_{CW})}{c} \quad (1.23)$$

$$t_{CCW} = \frac{R(2\pi + \Omega t_{CCW})}{c} \quad (1.24)$$

Solving separately for t_{CW} and t_{CCW} we find that to first order in $R\Omega/c$, the wave transit times differ by

$$\Delta t = t_{CW} - t_{CCW} = 4\pi \frac{R}{c} \left(\frac{R\Omega}{c} \right). \quad (1.25)$$

Usually the fiber is wrapped in a coil with N turns of radius R because this provides adequate sensitivity. For N turns Δt becomes;

$$\Delta t = t_{CW} - t_{CCW} = 4\pi \frac{RN}{c} \left(\frac{R\Omega}{c} \right) \quad (1.26)$$

Substituting coil length $L = 2\pi RN$ and coil diameter $D=2R$,

$$\Delta t = \frac{LD\Omega}{c^2} \quad (1.27)$$

Phase shift;

$$\Delta\phi = \omega \cdot \Delta t = \frac{\omega \cdot L \cdot D \cdot \Omega}{c^2}, \text{ where } \omega \text{ is angular frequency of light wave } \left(\frac{\omega}{c} = \frac{2\pi}{\lambda_{\text{vakum}}} \right).$$

Thus the Sagnac phase shift for light of wavelength λ in propagating through a coil of length L and diameter D is;

$$\boxed{\Delta\phi_s = \frac{2\pi \cdot L \cdot D \cdot \Omega}{\lambda \cdot c}} \quad (1.28)$$

The most important parameter for fiber optic gyroscopes is the gyro scale factor ($SF = \Delta\phi_s / \Omega$). [8]

$$\boxed{SF = \frac{2\pi \cdot L \cdot D}{\lambda \cdot c}} \quad (1.29)$$

1.2.2 Bias Modulation

The fiber-optic gyroscope provides an interference signal of the Sagnac effect, $\Delta\phi_s = \frac{2\pi \cdot L \cdot D \cdot \Omega}{\lambda \cdot c}$, with perfect contrast, since the phases as well as the amplitudes of both counter propagating waves are perfectly equal at rest. The optical power response is then a raised cosine function, $\langle P \rangle = \frac{I_0}{2}(1 + \cos\Delta\phi_s)$, of the rotation induces phase difference $\Delta\phi_s$, which is maximum at zero. To get high sensitivity, this signal must be biased about an operating point with a nonzero response slope:

$$\langle P \rangle = \frac{I_0}{2} [1 + \cos(\Delta\phi_s + \Delta\phi_b)], \quad (1.30)$$

where $\Delta\phi_b$ is the phase bias. $\Delta\phi_b$ must be as stable as the anticipated sensitivity; that is, significantly better than 1 μrad [6].

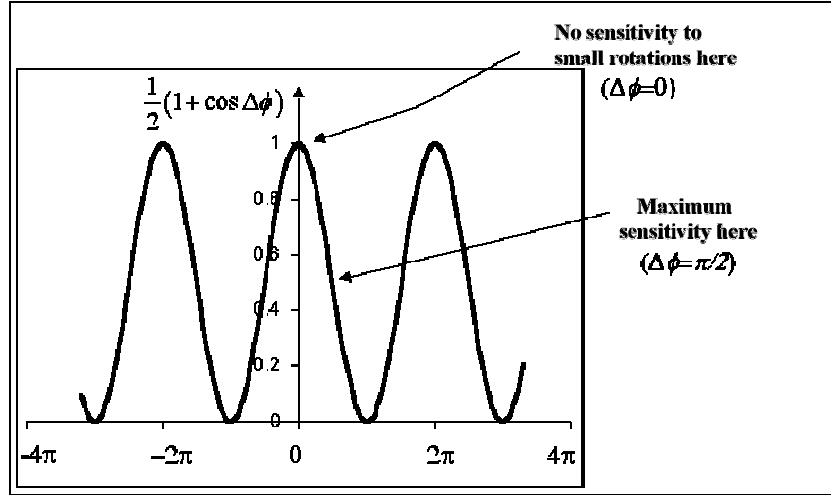


Figure 1.10. Sensitivity at various points on interferogram

The problem of drift of phase bias is completely overcome with the use of a reciprocal phase modulator placed at one end of the coil that acts as a delay line. Waves acquire phase shift $\phi_m(t)$ while passing through modulator at time t . Counter propagating waves pass through modulator at different times; while CW wave passes through modulator at time t , CCW wave passes through modulator at time $t - \tau$. Here τ is the loop transit time (nL/c). This yields a biasing modulation $\Delta\phi_m(t)$ of the phase difference:

$$\Delta\phi_m(t) = \phi_m(t) - \phi_m(t - \tau) \quad (1.31)$$

and the interference signal becomes

$$\langle P(t) \rangle = \frac{I_0}{2} \{1 + \cos[\Delta\phi_s(t) + \Delta\phi_m(t)]\} \quad (1.32)$$

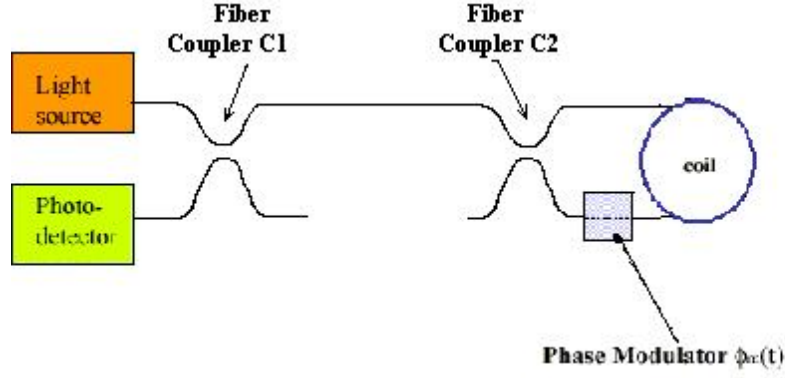


Figure 1.11. Method to inject relative phase shift between CW and CCW waves

There are various phase modulation mechanisms. One of them is electrooptic modulator. Wave acquires phase shift in passing through crystal with external voltage applied. Another is fiber wrapped around Piezoelectric Transducer (PZT). PZT stretches fiber when external voltage applied; lengthens optical path. Injected phase is proportional to applied voltage for both mechanisms.

Standard bias modulation technique is,

$$\phi_m(t) = \phi_0 \sin(\omega_m t) \quad (1.33)$$

So $\Delta\phi_m(t)$ becomes,

$$\Delta\phi_m(t) = \phi_0 [\sin(\omega_m t) - \sin(\omega_m t - \omega_m \tau)] \quad (1.34)$$

Using trigonometric identity: $\sin A - \sin B = 2 \cos\left(\frac{A+B}{2}\right) \cdot \sin\left(\frac{A-B}{2}\right)$,

$$\Delta\phi_m(t) = 2\phi_0 \cos(\omega_m t - \omega_m \tau/2) \sin(\omega_m \tau/2) \quad (1.35)$$

Defining constants to simplify: $\delta = \omega_m \tau/2$ and $\alpha = 2\phi_0 \sin \delta$,

$$\Delta\phi_m(t) = \alpha \cdot \cos(\omega_m t - \delta) \quad (1.36)$$

Now that the phase modulation term is known, returning to the detector signal

$$\begin{aligned}\langle P(t) \rangle &= \frac{I_0}{2} \{1 + \cos[\Delta\phi_s + \Delta\phi_m(t)]\} \\ &= \frac{I_0}{2} \{1 + \cos(\Delta\phi_s) \cos[\Delta\phi_m(t)] - \sin(\Delta\phi_s) \sin[\Delta\phi_m(t)]\}\end{aligned}$$

$$\langle P(t) \rangle = \frac{I_0}{2} \{1 + \cos(\Delta\phi_s) \cos[\alpha \cdot \cos(\omega_m t - \delta)] - \sin(\Delta\phi_s) \cdot \sin[\alpha \cdot \cos(\omega_m t - \delta)]\} \quad (1.37)$$

The harmonic contents of this signal is to be found using Bessel function identities.

$$\begin{aligned}\cos[z \cos(\theta)] &= J_0(z) + 2 \sum_{k=1}^{\infty} (-1)^k J_{2k}(z) \cos[2k\theta] \\ &= J_0(z) - 2J_2(z) \cos[2\theta] + 2J_4(z) \cos[2\theta] + \dots \\ \sin[z \cos(\theta)] &= 2 \sum_{k=0}^{\infty} (-1)^k J_{2k+1}(z) \cos[(2k+1)\theta] \\ &= 2J_1(z) \cos[\theta] - 2J_3(z) \cos[3\theta] + 2J_5(z) \cos[5\theta] + \dots\end{aligned} \quad (1.38)$$

Here $J_k()$ is k^{th} Bessel function of the 1st kind.

From the Bessel identities above, it can be seen that

* $\sin[\Delta\phi_m(t)]$ terms give odd harmonics of ω_m

* $\cos[\Delta\phi_m(t)]$ terms give even harmonics of ω_m

Frequency content of detector signal is

$$\langle P(t) \rangle = \frac{I_0}{2} \times \left\{ \begin{array}{l} 1 + J_0(\alpha) \cos(\Delta\phi_s) \quad \leftarrow \text{DC} \\ -2J_1(\alpha) \sin(\Delta\phi_s) \cos[\omega_m t - \delta] \quad \leftarrow \text{1st harmonic} \\ -2J_2(\alpha) \cos(\Delta\phi_s) \cos[2(\omega_m t - \delta)] \quad \leftarrow \text{2nd harmonic} \\ +2J_3(\alpha) \sin(\Delta\phi_s) \cos[3(\omega_m t - \delta)] \quad \leftarrow \text{3rd harmonic, vs...} \\ +\dots \end{array} \right. \quad (1.39)$$

Signal at modulation frequency is

$$\left\langle P(t) \right\rangle_{\omega_m} = -I_0 J_1(\alpha) \cdot \sin(\Delta\phi_s) \cdot \cos[\omega_m t - \delta] \quad (1.40)$$

Detector signal contains all harmonics of ω_m but desirable part is at 1st harmonic of ω_m . In order to extract signal at ω_m only, Lock-in Amplifier (LIA) can be used.

- * If $\Delta\phi_s = 0$, signal vanishes.
- * For $\Delta\phi_s \ll 1$, signal $\approx \sin \Delta\phi_s \approx \Delta\phi_s$
- * Signal polarity reverses when rotation direction switches ($\Delta\phi_s \rightarrow -\Delta\phi_s$).

Comparing to unmodulated signal;

- * Unmodulated signal $\approx (1 + \cos \Delta\phi) \approx \Delta\phi_s^2$ for $\Delta\phi_s \ll 1$.
- * Sign of unmodulated signal independent of rotation direction.

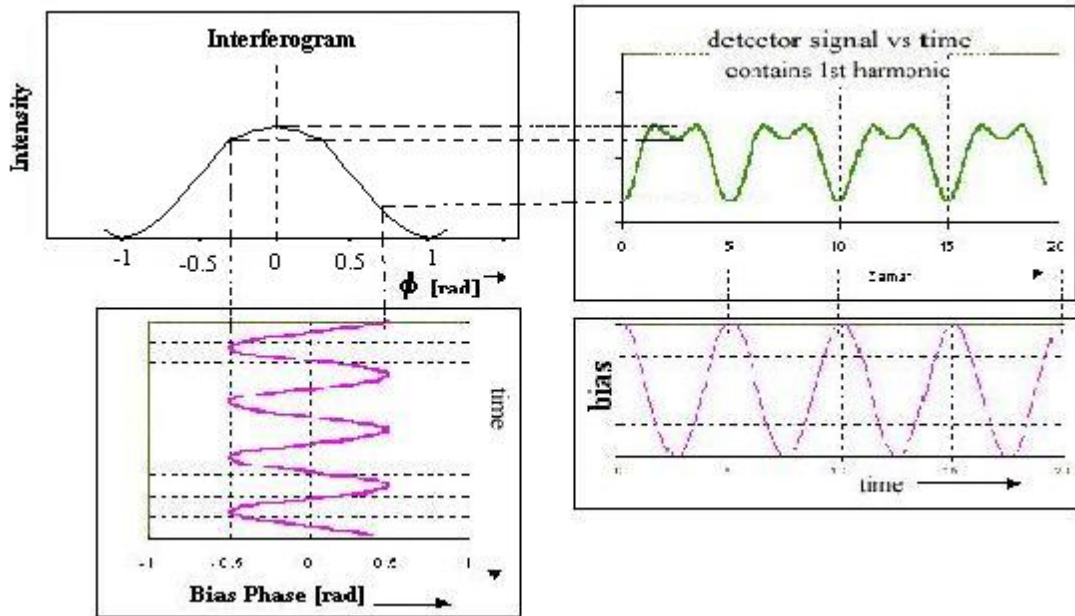


Figure 1.12. Sinusoidal bias modulation: detector signal with finite Sagnac phase shift [9]

CHAPTER 2

FOG CONSTRUCTION AND COMPONENTS

2.1 Reciprocity

System configuration may cause a non-reciprocal phase shift different from Sagnac phase shift. This phase shift could dominate Sagnac phase shift because the Sagnac shift is so small. To accurately measure the Sagnac phase difference it is necessary to reduce other phase differences which can vary under the influence of the environment. The degree to which this is possible determines the quality of the gyroscope. This problem can be solved very simply with a “reciprocal configuration”[6]. To achieve this high sensitivity, the optical paths traveled by the two beams must be identical when the gyro is not rotating, so the system must be reciprocal. Having propagated through the same optical path the two waves have, in the absence of nonreciprocal effects, the same phase delay. Variations of the system by the environment changes the phase of both waves equally so no difference in the phase delay results. In this way, the system obtains a basic degree of immunity to environmental influences [10-11].

As it is seen from the *Figure 2.1*, CW and CCW waves travel identical paths, in opposite directions: CW wave passes through BS1, passes through BS2 to enter loop, crosses BS2 to exit loop and crosses BS1 to enter photo detector; CCW wave passes through BS1, crosses BS2 to enter loop, passes through BS2 to exit loop and crosses BS1 to enter photo detector. Both waves pass through phase modulator at opposite ends of journey.[9]

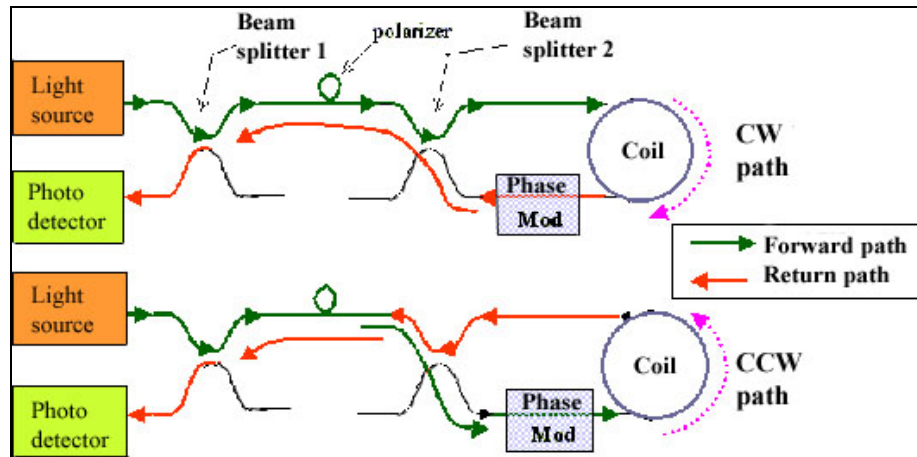


Figure 2.1. Reciprocal configuration

Maintaining reciprocity on a scale sufficient to ensure proper operation of the gyroscope is not so simple. There are only a few nonreciprocal effects: nonlinear interactions, magnetic phenomena, time-varying phenomena, and relativistic phenomena. The Sagnac effect is relativistic, and is exploited for this device. The other undesired effects must be minimized [12]. If medium is linear, time-invariant and free of magnetic fields, then CW and CCW optical path lengths are identical and the two waves return to detector perfectly in phase, except for Sagnac shift.

Fiber structure is slightly anisotropic: Optical path length and refractive index is different for waves with orthogonal polarization states. If both polarization states propagate through loop, then some waves interfere at detector with birefringence phase shift rather than Sagnac phase shift. So polarizer is inserted into optical path to solve this problem.

Optical fiber waveguide allows discrete guided spatial modes. Different spatial modes travel with different group velocity. If two spatial modes interfere at detector, then relative phase difference is due to differential velocity of the spatial modes, rather than Sagnac phase shift. The solution of this problem is using fiber that guides only a single spatial mode [9].

2.2) Fiber Coil

Fiber coil is the most important part of Sagnac Interferometer, so does fiber optic gyroscopes. Sagnac phase shift is proportional to product of coil length and diameter. Mechanical and thermal characteristics of fiber coil are important for fiber optic gyroscopes. Time-varying thermal or mechanical stress causes bias error. In addition, gyro scale factor varies with coil dimension. In section 3.1, it is said that the CW and CCW waves travel reciprocal paths if the fiber medium is time-invariant. However, if fiber properties are time-varying, e.g., expanding/contracting fiber, CW wave encounters variation at time t while CCW wave encounters variation at different time, $t-\delta t$. Consequently a nonreciprocal phase shift exist, even if absence of rotation which is a gyro error. It is obvious that, fiber characteristics are important for fiber optic gyroscopes. The fiber used in fiber optic gyroscope must have some characteristics. First, it must be single spatial mode because different modes have different propagation velocities. Second, the fiber medium must be linear. If it is nonlinear, Kerr effect error occurs. Third, fiber diameter must be large because thermal phase noise worse for small fiber diameter and the last, loss in fiber must be low because the ratio of signal to shot noise proportional to $(\text{detector power})^{1/2}$. As a result, coils must be carefully wound to minimize thermal & stress gradients, asymmetries, and dynamic responses. [9] (For detailed information see reference [6])

2.3) Light Source

There are few constraints on the source for a fiber optic gyroscope. Probably the most obvious is that it must be able to inject a significant amount of optical power, e.g., 100 μW or more, into a single-mode waveguide. Another restriction on the source is set by noise due to Rayleigh backscattered light in the fiber. This has been reduced primarily by reducing the coherence length of the source light. To achieve current state-of-the-art short-term levels, it appears that the source coherence must be less than, or approximately, 1 cm. Wavelength stability is another restriction

on the source because of the scale factor which is proportional to mean wavelength [10].

Laser diode (LD) have high output power and coupling efficiency, but their coherence is strong, and with a narrow optical spectrum width.

Light-emitting diodes (LED) have advantages of broad optical spectrum and small coupling noises, but its output power and coupling efficiency are low.

Superluminescent diode (SLD) has high output power and a broad optical spectrum width. It characterizes between LD and LED. It may suppress nonreciprocal phase shift owing to Rayleigh scattering noise and nonlinearity Kerr effect. SLD is an ideal light source for fiber optic gyroscope.

Advantages of SLD are being all-solid state, requiring low drive voltage, having broad bandwidth ($\Delta\lambda \sim 20$ nm at $\lambda \sim 850$ nm) and short coherence length ($L_c \sim 6$ μm).

Disadvantage of SLD is having poor wavelength stability (400ppm/ $^{\circ}\text{C}$ temperature dependence and 40 ppm/mA drive current dependence) [13],[15].

Rare earth-doped fiber light source (FLS) is the other source used in fiber optic gyroscope. To overcome the problem of SLD wavelength stability, FLS has been developed. FLS has more complex configuration but this source is more useful than SLD.

Advantages of FLS are having excellent wavelength stability possible, high output power, unpolarized output that reduces polarization error, light generated within SM fiber easily couples to fiber gyro and shapeable spectrum.

Disadvantage of FLS is having long coherence length ($L_c \sim 200$ μm) [14-16].

2.4) Coupler

Coupler functions in gyroscopes can be described as:

- Coupler 1 (“source” coupler)
 - direct source light to gyro loop on forward path
 - direct returning light to detector

- Coupler 2 (“coil” or “loop” coupler)
 - Separate light into CW and CCW waves to traverse loop
 - Recombine CW and CCW waves after loop [9]

Consider perfectly matched interferometer with 50-50 splitter at entrance/exit.

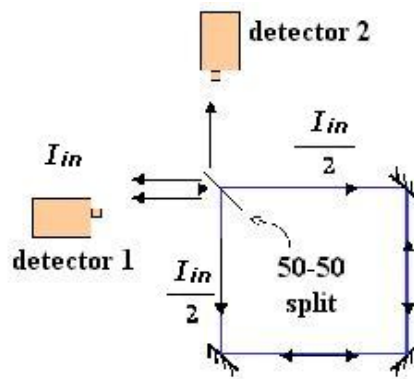


Figure 2.2. Reciprocal use of coupler

At detector 1:

Both CW and CCW waves are transmitted once and reflected once. Beams are traveled identical paths so $\Delta\phi_1 = 0$.

$$\langle P_1 \rangle = \frac{I_{in}}{4} + \frac{I_{in}}{4} + 2\sqrt{\frac{I_{in}}{4} \frac{I_{in}}{4}} \text{Cos}\Delta\phi_1 = I_{in}$$

At detector 2:

Reflected wave has 90° phase shift relative to through wave so the phase shift between CW and CCW waves is $\Delta\phi_2 = 180^\circ$. Therefore, the power detected here is $\langle P_2 \rangle = \langle P_1 \rangle - I_{in} = 0$. [6] This is true of cross-coupled and transmitted waves in a coupler. Reciprocal configuration ensures both waves are transmitted/cross-coupled equal number of times [9].

2.5) Phase Modulators

There are two widely used varieties of phase modulator:

a) *Piezoelectric Transducer:*

Fiber is wrapped around piezoelectric tube. This tube expands in response to drive voltage, stretching fiber and increasing optical path length. However, this modulator is limited to low modulation bandwidth (~ 100 kHz). [9]

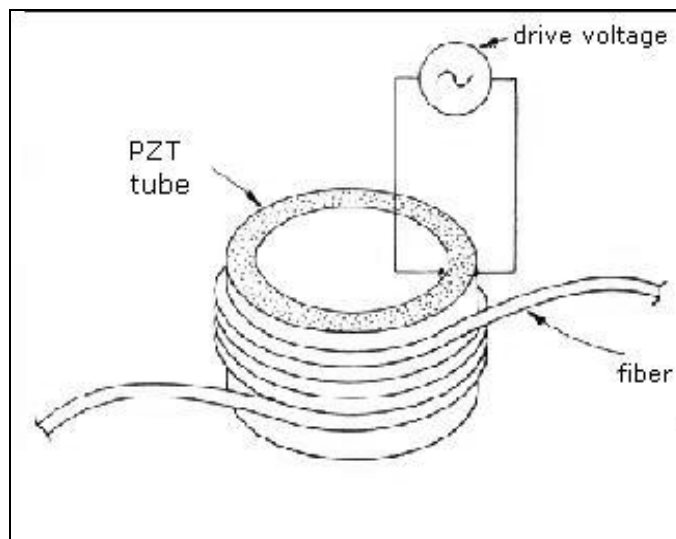


Figure 2.3. PZT modulator [6]

b) Electro-optic Modulator:

Light propagates through electro-optic waveguide. Electrodes placed adjacent to waveguide allow electric field application. Electric field modifies waveguide dielectric character, including optical phase shift. This kind of modulation has very high bandwidth (>100MHz). [9]

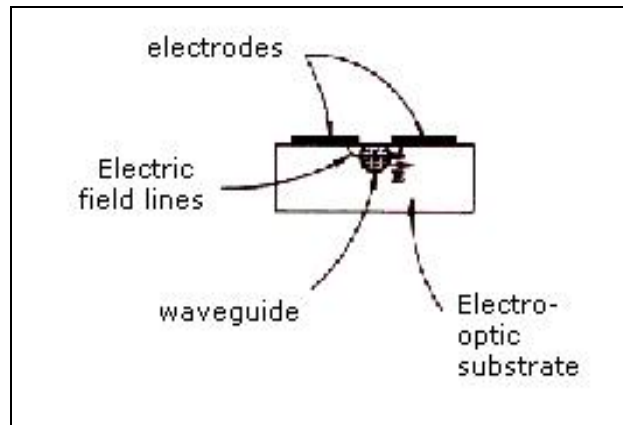


Figure 2.4. Electro-optic modulator [6]

2.6) Detector

Detector characteristics are important for fiber optic gyroscopes. Detector must have high quantum efficiency (electrons created per photon absorbed), low drive voltage, small size, stable gain over environment conditions (e.g., temperature).

Possible detectors used in fiber optic gyroscope:

a) Photomultiplier tube:

This is almost never used in gyroscopes because of poor quantum efficiency (especially in infrared), large physical size, high bias voltage (~1kV) required.

b) *Avalanche photodiode:*

This is seldom used in gyroscopes because of temperature-dependent gain, non-optimum noise contribution and ~100V bias voltage required.

c) *PIN diode:*

This is widely used in gyroscopes. Advantages of this detector are excellent size and noise characteristics, good environmental stability and low cost [9].

CHAPTER 3

GYRO PERFORMANCE

Gyro performance depends on some conditions. These conditions are noise, bias stability, input axis alignment, deadzone, scale factor.

3.1 Noise

The ideal performance of an optical gyroscope is limited by noise. The output of the gyro is converted into an intensity variation that a detector measures. Any change in intensity due to noise can not be distinguished from a change in intensity due to rotation. Therefore, the uncertainty in rotation rate is determined by the level of noise in the system.

3.1.1 Shot Noise

Intensity changes due to source variation can be referenced out, but fluctuations due to shot noise cannot be reduced, as they arise from a random process. This is because of statistical fluctuations in photon flux at detector. The uncertainty in the actual phase signal is given by

$$\delta\phi = \frac{\text{photon shot noise}}{\text{fringe slope}}. \quad (3.1)$$

Plugging this into the sensitivity of a fiber gyro, the ultimate rotation uncertainty is

$$\delta\Omega = \frac{\lambda c}{4\pi RL} \delta\phi. [12] \quad (3.2)$$

3.1.2 Johnson Noise

This occurs because of fluctuations in current across resistor due to thermal motions of electrons within resistor.

3.1.3 Thermal Phase Noise

Thermal fluctuations occur in optical refractive index of fiber. This causes noise.

3.1.4 Relative Intensity Noise

This occurs because of beating of separate wavelengths within finite bandwidth light spectrum[9] (For detailed information on noise see [12], [17], [18])

3.2. Bias Stability

When a gyro indicates finite rotation rate, even in the absence of true rotation rate, the gyro is said to have a 'bias offset' or simply 'bias'. Bias is not problematic if it is stable. It can be calibrated and subtracted. However, mechanisms that produce bias offset are generally not stable. Reciprocal gyro configuration makes interferometer insensitive to environment but bias error mechanisms do not satisfy reciprocity.

3.2.1 Bias Error Mechanisms

3.2.1.1. Modulator Error

Modulator error is produced by modulator. There are two kinds of modulator error:

3.2.1.1.a) Nonlinearity

For an ideal modulator, optical phase shift strictly proportional to applied voltage but for an imperfect modulation, optical phase shift responds nonlinearity to

voltage. This nonlinearity generates spurious second harmonic phase modulation and creates spurious detector signal synchronous with phase modulation.

This problem can be eliminated by designing nearly perfect modulator, or adjusting modulation frequency ω_m at proper frequency ω_p in order to vanish the second harmonic term.

$$\omega_m = \omega_p = \pi/\tau \quad (3.3)$$

3.2.1.1.b) Intensity Modulation

Another modulator-induced bias error mechanism is intensity modulation. Modulator applies time varying phase and attenuation to optical waves. Thus, intensity modulation by the modulator produces a bias error which varies with environment (e.g., temperature). This error also vanishes at proper frequency ω_p .

3.2.1.2 Secondary waves

As it is said before, detector signal measures phase shift between ‘primary’ CW and CCW waves, which are forced to travel reciprocal paths. However other ‘secondary’ waves also propagate through gyroscope [see Clifford]. They do not travel reciprocal paths. Backscattered waves and polarization cross-coupled waves are two examples of these waves. These are sources of bias instability.

3.2.1.3 Nonreciprocal Effects

It is assumed that primary waves are reciprocal if they travel the same physical path. This is not always true. Reciprocity is broken in some situations:

Shupe Effect:

If fiber properties vary with time, CW and CCW waves see fiber properties at different time [22].

Kerr Effect:

If fiber properties are nonlinear, thus refractive index depends on electric field amplitude; CW and CCW waves have different amplitudes [23].

Faraday Effect:

Magnetic field breaks CW-CCW symmetry.

3.3 Input Axis Alignment

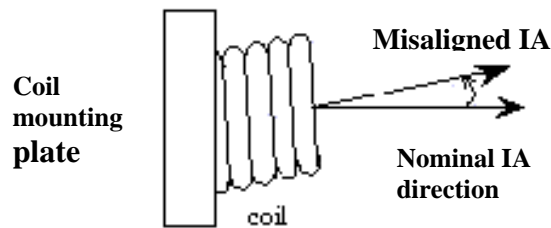


Figure 3.1. Input axis alignment

Misalignment of input axis can result in two kinds of apparent errors:

1) Scale factor error:

This occurs when there is rotation about the nominal IA axis. Consider rotation rate Ω about the nominal IA direction. In this case, coil sees rate fraction $\Omega \cos \theta$ Then indicated rate error is

$$\Delta\Omega = \Omega \cdot (1 - \cos \theta) \approx \frac{\Omega \theta^2}{2} \quad (3.4)$$

and apparent scale factor error is

$$\frac{\Delta\Omega}{\Omega} = \frac{\theta^2}{2} \quad (3.5)$$

2) Bias Error:

This occurs when there is rotation about an orthogonal axis. Consider rotation rate Ω about an axis perpendicular to nominal IA. Spurious rate seen by coil is

$$\Omega_{error} = \Omega \cdot \sin \theta \approx \Omega \theta \quad (3.6)$$

this appears as bias error in absence of rotation about nominal IA axis.

Careful mechanical packaging is the solution to IA instability.

3.4 Deadzone (Lock-in)

Deadzone is the region of low rotation rates within which gyro indicates exactly zero rotation.

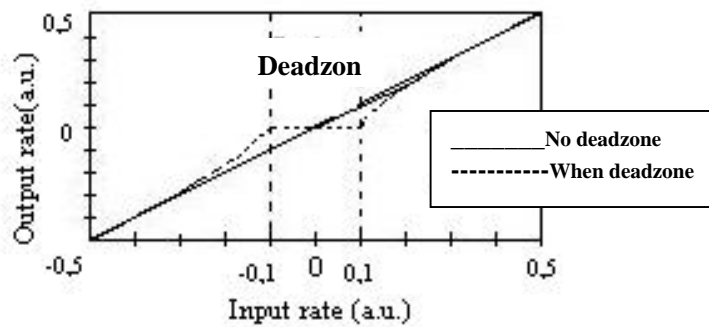


Figure 3.2. Transfer functions for an ideal fiber gyro and for a fiber gyro with deadzone

3.5 Scale Factor Stability

Scale Factor (SF) is the ratio of gyro output per unit rotation rate. SF is expected to be perfectly constant. Thus, gyro signal should increase linearly with rotation rate. One can achieve scale factor stability if this condition is achieved. [9]

CHAPTER 4

SIMULATION ON

INTERFEROMETRIC FIBER OPTIC GYROSCOPE

WITH AMPLIFIED OPTICAL FEEDBACK (FE_FOG)

4.1 Properties of the Simulation Program, VPItransmissionMaker™

Simulation Program VPItransmissionMaker enables the user to prepare and configure photonic simulations on her/his computer. VPItransmissionMaker can fully verify link designs at a sampled-signal level to identify further cost savings, investigate novel technologies, or fulfill specialist requirements. Links can be automatically imported from VPIlinkConfigurator for detailed design and optimization. VPItransmissionMaker is widely used as an R&D tool to evaluate novel component and subsystems designs in a systems context, investigate and optimize systems technologies (e.g. coding, modulation, monitoring, compensation, regeneration). VPIcomponentMaker™ allows active and passive devices, and optical amplifiers to be designed, and their performance abstracted for systems-level simulations with VPItransmissionMaker™. New amplifier technologies (multistage, multipump, hybrid and waveguide) can be developed, optical signal processing (wavelength conversion, clock recovery, partial regeneration) investigated, and the performance of lasers and tunable lasers in conjunction with integrated modulators can be assessed [21].

Sophisticated design tool for photonic devices, components, systems and network are developed. Tools must support signal representations and algorithms for modeling optical components and network elements at different level of abstraction.[20]

4.2 Signal Representations

Data exchange can be organized in blocks or by transmitting individual samples. The Block Mode is more suitable for systems simulations where components are widely-spaced compared with the modeled time, or where signals flow unidirectionally, from transmitter to receiver. This is the most efficient form of simulation, as modules are only ‘fired’ when data passes through them.

Passing data between modules on a sample-by-sample basis is necessary when delay between the modules is much shorter than a block length: the modules must communicate rapidly in order to fully simulate their joint behavior. A good example of an application of Sample Mode is the stabilization of lasers using external cavities. The cavity and laser have to be simulated simultaneously (and fire at each iteration) in order to determine the optical spectrum of the compound cavity and its modulation dynamics.

Because of bidirectional signal flow and delay between the modules is important in fiber-optic gyros, Sample Mode signal representation must be used in the simulation. [20]

4.3 Global Variables

The default Global Variables are:

TimeWindow:

This sets the duration of the blocks in seconds. For simulations the **TimeWindow** must be set so the block contains 2^m , (m integer) data bits. This is achieved by setting

$$\mathbf{TimeWindow} = 2^m / \mathbf{BitRateDefault}$$

Because *VPltransmissionMaker* parameters can be expressions, a valid input is therefore

$$\mathbf{TimeWindow} = 128.0 / 2.5e9 \text{ for 128-bits at 2.5 Gbit/s.}$$

A long time window leads to greater simulation accuracy (*e.g.* in BER estimation, or in spectral resolution), but increases computation time.

BoundaryConditions:

This parameter sets whether the data within a block is considered to be *periodic* or *aperiodic*. If it is *periodic*, then all frequency components are considered to be exact harmonics of $1/\text{TimeWindow}$. It has several advantages when modeling dispersive nonlinear optical fibers. If the Boundary Conditions are *aperiodic*, the data in successive blocks is 'stitched'¹ together. This is useful for modeling components with long time constants compared with the bit-rate, such as semiconductor lasers, because visualizers are updated every block, but the simulation and the laser dynamics extend over several blocks. Using aperiodic boundary conditions requires the aperiodic fiber model.

SampleRateDefault:

The modules where the parameter

$$\mathbf{SampleRate} = \text{SampleRateDefault}$$

will use the value of **SampleRateDefault** which is given a value in the Global Variables. This is a useful technique when all transmitters are using the same sample rate, as the sample rate can be set with the single global variable. For digital simulations, the sample rate of each module must be a power of two multiple of the **BitRate**. That is:

$$\mathbf{SampleRate} = 2^m \cdot \mathbf{BitRate} \text{ (where } m \text{ is an integer)}$$

Because the Parameter Editor accepts expressions, this can be entered easily, for example **SampleRate** = $16 \cdot 2.5e9$, gives an optical bandwidth of 16 times 2.5Gbit/s [20].

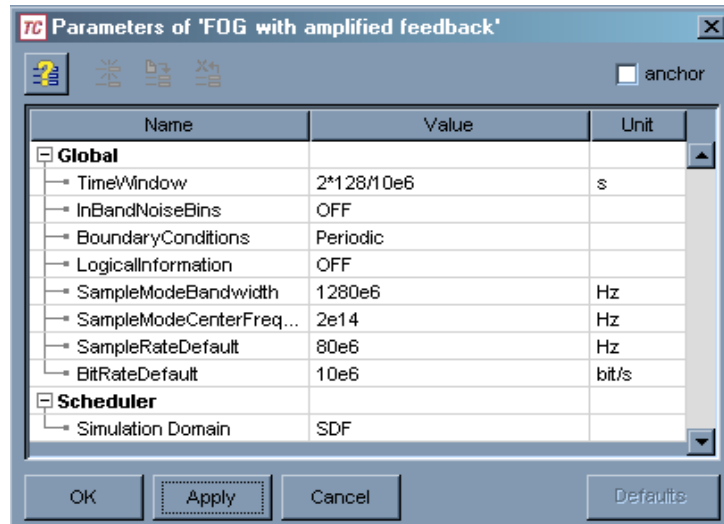


Figure 4.1. Global parameters

4.4 Interferometric Fiber Optic Gyroscope with Amplified Optical Feedback (FE_FOG)

Interferometric Fiber Optic Gyroscope with Amplified Optical Feedback (FE_FOG) is based on multiple utilization of the Sagnac loop through feedback of a part of the output signal into the input port. This fiber gyroscope functions like a resonant fiber optic gyroscope (R_FOG). R_FOG consists of a recirculating passive optical cavity [24-25]. The change in the resonance frequency of the counterpropagating waves is transformed into a variation of the output power. This system faces a very difficult problem: to fully exploit the system, a very narrow source spectrum is required, and the related large coherence length induces various sources of noise, which degrade the performance. FE_FOG is a different kind of gyroscope because a low-coherence light source is used and there is no resonant effect in the FE_FOG. Therefore, FE_FOG has a simple structure when compared with an R_FOG. The important characteristics of the FE_FOG is that it works in the pulse state, and the rotation can be measured by detection of the output pulse. The sensitivity of the gyroscope is enhanced and the dynamic range is improved when compared with the ordinary interferometric fiber optic gyroscope [19].

4.5 Configuration of a FE_FOG

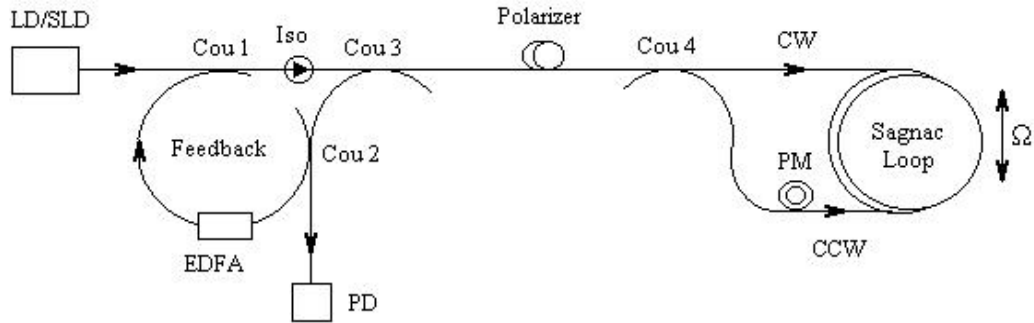


Figure 4.2. Configuration of the FE_FOG

Figure 4.2 illustrates the basic configuration of the FE_FOG. The CW's and CCW waves of each round trip interfere at the output, and the total output is the summation of each interference. Because low-coherence light is used, the resonant effect does not occur. Only the summation of the interferences for each round trip is produced because of the optical feedback.

A more detailed description of Figure 4.2 is as follows:

A low coherence light source LD or SLD is used, and light input travels into the Sagnac loop through couplers (cou's) 1, 3, and 4. The interference signal is also received through couplers 4 and 3, of which coupler 4 is an interferometric coupler. Here, to keep optical reciprocity, two couplers, 3 and 4, is used. The output signal is then fed into coupler 2; one part of the rotation signal is received by the photodetector (PD), another part is fed back into the sensing loop through feedback couplers 2 and 1. In addition, an isolator is used for two functions. First, it can support only a one-direction operation for the optical feedback. Second, it can stop the light that returns back to the light source, which may induce additional noise. It should be mentioned that there is no Sagnac phase change in the fiber amplifier loop because the optical isolator produces light propagation in only one direction.

In this system, the weak feedback signal is amplified by a fiber amplifier (EDFA). However, the gain of EDFA must be adjusted properly so that there is no laser emission. In addition, it is assumed that the fiber amplifier is operating in a linear mode so there are no power-level effects.

The total output signal is a summation of the interference of CW and CCW waves for each round trip. Because a phase modulator is placed within the Sagnac loop, the total output signal is a series of short pulses if the frequency of phase modulator is selected properly. To realize pulse operation, modulation frequency of the phase modulator and round-trip-time delay must be selected to satisfy a relation of $\omega_m \tau = 2n\pi$ where ω_m is the angular frequency of the phase modulation and τ is the time delay of the light through the whole round trip, which includes the Sagnac-loop plus the fiber-amplifier delay. If there is deterioration in the pulse shape as the modulation becomes detuned, it can be more or less compensated by a variation of the EDFA gain. The sharpness of the output pulse can be obtained by an adjustment of the feedback couplers and the fiber amplifier. In addition, it should be noted that the gain of EDFA is a function of the wavelength. Therefore, the wavelength stability of the low-coherence light source is expected. Indeed, the wavelength stability of the light source is the key issue for the scalar factor in any fiber optic gyroscope [19].

4.6 Theory

The first time interference signal without feedback has the same form as in that in the ordinary interferometric fiber optic gyroscope, which is expressed as

$$P_1(t) = K_1 \{1 + v \cos[\phi_s + \phi_e \cos(\omega_m t)]\}, \quad (4.1)$$

where v is the interferometric coefficient, which is a parameter of fringe contrast, and K_1 is a parameter that express the loss resulting from the Sagnac interferometer,

ω_m is the modulation frequency ($\omega_m = 2\pi f_m$), ϕ_e is the effective phase modulation depth, which is expressed as

$$\phi_e = 2\phi_m \sin(\pi f_m \tau_s), \quad (4.2)$$

τ_s is the wave propagation time through the Sagnac loop and expressed as $\tau_s = nL/c$ where L is the length of the loop, and ϕ_m is the phase-modulation depth. ϕ_s is the Sagnac phase shift induced by rotational movement, which is expressed as

$$\phi_s = 4\pi RL\Omega / \lambda_0 c. \quad (4.3)$$

Here Ω is the rotation rate, R is the radius of the Sagnac loop, and c is the velocity of light propagation in free space.

Considering the effect of optical feedback, the second-time interference signal experienced after the feedback has been derived is

$$P_2(t) = AK_1K_2 \{1 + \nu \cos[\phi_s + \phi_e \cos(\omega_m t - \omega_m \tau)]\} \times \{1 + \nu \cos[\phi_s + \phi_e \cos(\omega_m t)]\} \quad (4.4)$$

and the third-time interference signal that occurs after feedback has been twice derived is

$$\begin{aligned} P_3(t) = & A^2 (K_1^3 K_2^2)^2 \{1 + \nu \cos[\phi_s + \phi_e \cos(\omega_m t - 2\omega_m \tau)]\} \\ & \times \{1 + \nu \cos[\phi_s + \phi_e \cos(\omega_m t - \omega_m \tau)]\} \\ & \times \{1 + \nu \cos[\phi_s + \phi_e \cos(\omega_m t)]\} \end{aligned} \quad (4.5)$$

where A is the gain of the fiber amplifier and K_2 is a parameter that depends on the coupling ratio of the feedback couplers and the transmission loss in the feedback loop. For simplicity, it is assumed that $K' = K_1 K_2$. The total output at the

photodetector is the summation of the number of above-mentioned interferences and is expressed as

$$P_{total}(t) = P_1(t) + P_2(t) + P_3(t) + K . \quad (4.6)$$

If $\omega_m \tau = 2n\pi$, the total photodetector output can be realized by proper adjustment of the modulation frequency to match the round-trip time, and $P_{total}(t)$ is

$$P_{total}(t) = \frac{K \{1 + \nu \cos[\phi_s + \phi_e \cos(\omega_m t)]\}}{1 - AK' \{1 + \nu \cos[\phi_s + \phi_e \cos(\omega_m t)]\}} , \quad (4.7)$$

where K is the photodetecting coefficient.

Because the total output is a series of short pulses, the peak value can be determined through the following equation:

$$P'_{total}(t) = 0 . \quad (4.8)$$

Thus,

$$K \nu \sin[\phi_s + \phi_e \cos(\omega_m t)] = 0 , \quad (4.9)$$

and

$$[\phi_s + \phi_e \cos(\omega_m t)] = 2n\pi , \quad n=0,1,2,\dots \quad (4.10)$$

This is the condition required to find the peak position of the output pulse that is valid for both cases of rotation and nonrotation. From this equation and condition it can be seen that the output pulse shifts if rotation occurs. This characteristic can be utilized for the rotation measurement [19].

4.7 Simulations and Discussions on FE-FOG

The simulation on interferometric fiber optic gyroscope with amplified optical feedback is performed. The schematic of the simulation is seen in the Figure 4.3. In the simulation, light cannot propagate through the fiber and modulator bidirectionally. So two fibers and phase modulators having the same properties added to CW and CCW wave paths. As it is said before, when gyro rotated, phase shift is induced between CW and CCW waves. In this simulation, the system cannot be rotated. So, phase shift must be added externally between two waves. The important point here is while phase shift on one wave is positive; the phase shift on the other wave must be negative. It is seen like that the two waves propagates through different pats. However, this is not violate the reciprocity because properties of these components are the same so, these two waves see exactly the same conditions. There is no need to insert an isolator in the system here because light propagates through the components unidirectionally. The only difference between actual configuration of gyroscope and the simulation is light source. Superluminescent Light Diode (SLD) must be used in the gyro but in the simulation program this component does not exist, so the Laser CW light source is replaced with SLD.

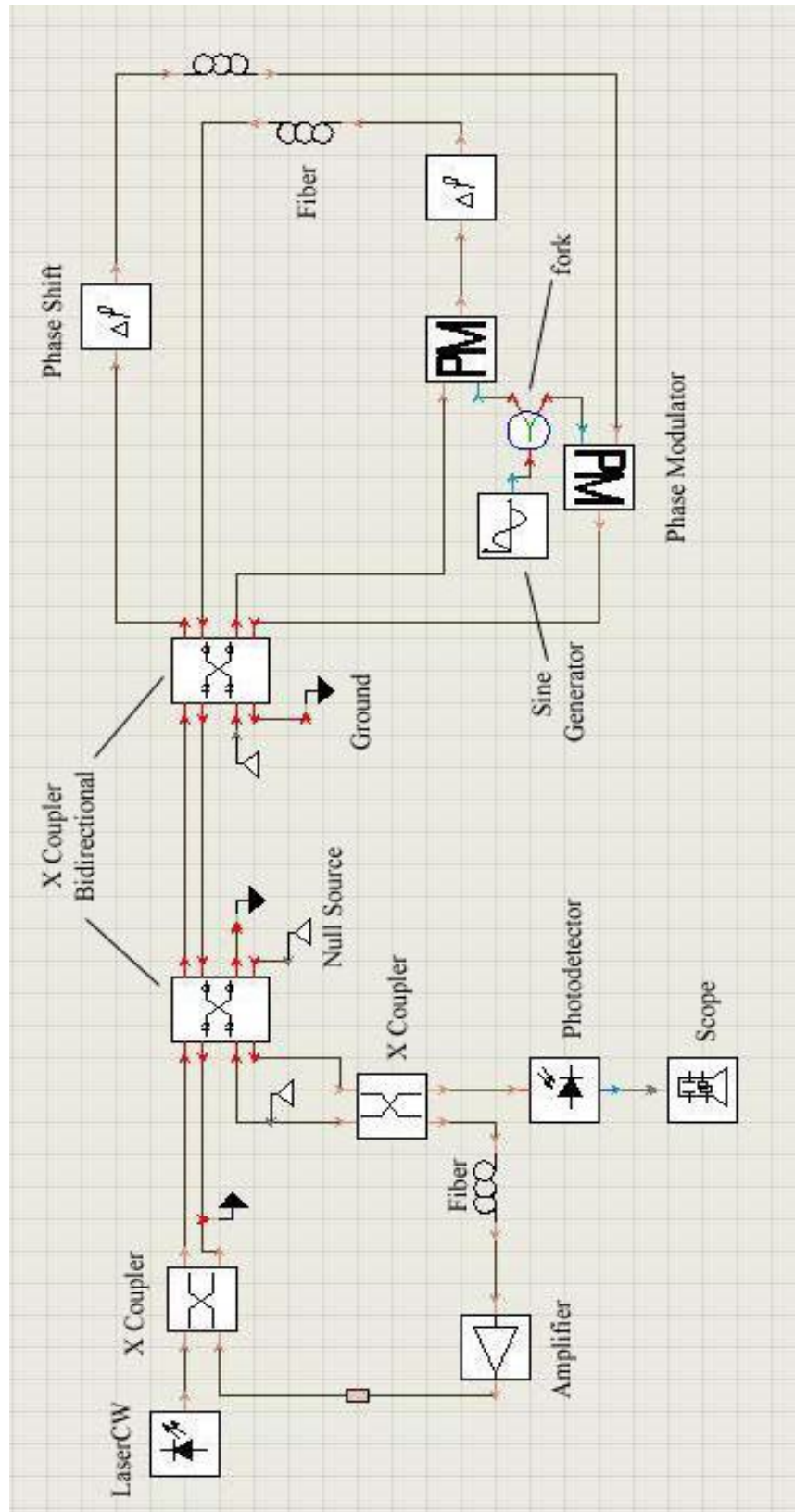


Figure 4.3. Schematic of the simulation

4.8 Modules Used in the Schematic*

4.8.1 LaserCW

LaserCW is used as a light source in the schematic. The module produces a continuous wave (CW) optical signal. The parameters of the module are shown in the Figure 4.4.

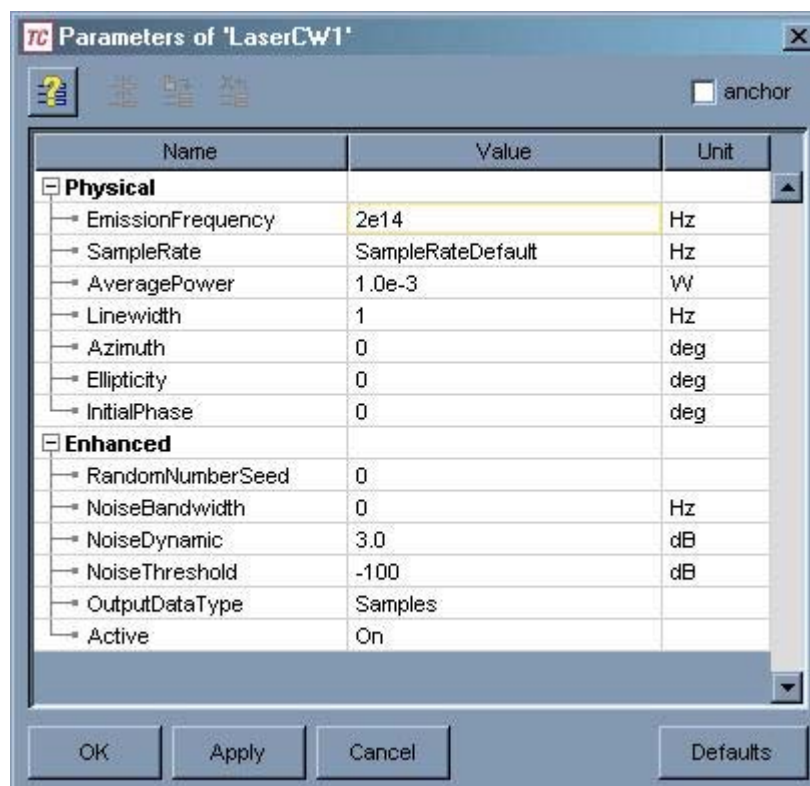


Figure 4.4. Parameters of LaserCW

* For detailed information see Appendix A.

4.8.2 X Coupler and X Coupler Bidirectional

X Coupler models an optical coupler for combining or splitting of optical signals. X Coupler Bidirectional acts as a bidirectional X Coupler.

In simulation **CoupleFactor** default parameter 0,5 is used for both couplers.

4.8.3 Phase Shift

The module adds a time-independent phase advance to the optical input signal. This module is used for simulating the Sagnac phase shift.

The parameter **PhaseShift** has changed several times and we got the solutions for each value.

4.8.4 Sine Generator (Electrical)

This module is used for bias modulation It generates an electrical sine waveform superimposed on a constant bias..

The parameters of the module are illustrated in Figure 4.5.

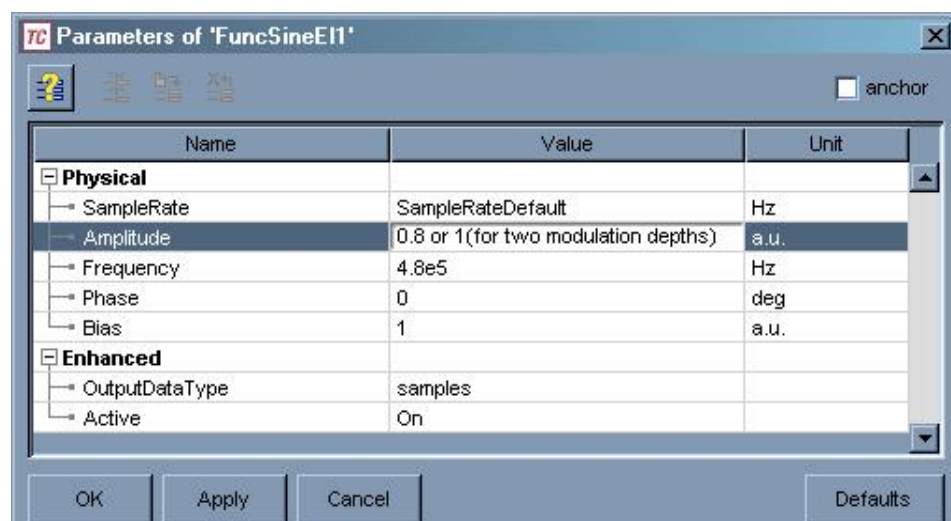


Figure 4.5. Parameters of Sine Generator

4.8.5 Multiple Output Connector (Fork)

This module copies input particles to each output.

4.8.6 Modulator Phase

Phase modulator is also used for bias modulation. The module simulates an ideal phase modulator (PM).

The only parameter PhaseDeviation for PM was taken 180 deg.

4.8.7 Photodiode (PIN)

The module acts as a PIN photodiode with additive Gaussian white noise sources.

In our simulation, parameters of PIN photodiode are shown in Figure 4.6.

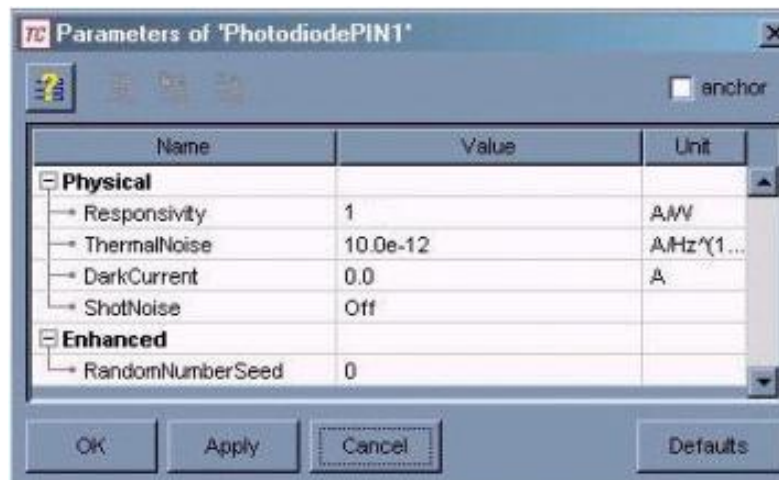


Figure 4.6. Parameters of Photodiode PIN

4.8.8 Time Domain Fiber

The only fiber used for Sample Mode signal is Time Domain Fiber. Three fibers used, two of them in Sagnac loop having the same parameters and the other one is placed in the feedback loop.

The parameters are shown in the Figure 4.7.

Name	Value	Unit
Physical		
Attenuation	0.05e-03	dB/m
AttenuationSlope	0.0e+09	dB/m ²
AttenuationSecondDeriv	0.0e+18	dB/m ³
Length	560	m
StepSize	90	m
Dispersion	16e-6	s/m ²
DispersionSlope	0.08e3	s/m ³
NonLinearIndex	2.6e-20	m ² /W
CoreArea	80.0e-12	m ²
Tau1	12.2e-15	s
Tau2	32.0e-15	s
RamanCoefficient	0.0	
Numerical		
Algorithm	Overlapadd	
Tolerance	0.001	
MaxFilterOrder	8	
MinFilterOrder	2	
MinImpulseLength	512	
StepFilterOrder	2	
MaxRunLength	5	
MaxPhaseRange	3.14159	
TargetError	1.0	degree
MaxFrequency	3.14159/2	
MinFrequency	-3.14159/2	
FrequencyStep	0.15	
Enhanced		
SignalType	Samples	
PhaseFitDump		
Options		

Figure 4.7. Parameters of the Time Domain Fiber in Sagnac Loop

The other fiber placed in the feedback loop has the same parameters except for **Length** and **StepSize** which is 40 m.

4.8.9 Ideal Amplifier with Wavelength Independent Gain

This module is used to amplify the feedback signal. It simulates a system-oriented amplifier with a wavelength-independent gain and noise Figure. By parameter selection the module may act in a gain-controlled, output power-controlled, or saturating (uncontrolled) mode.

The parameters are shown in the Figure 4.8.

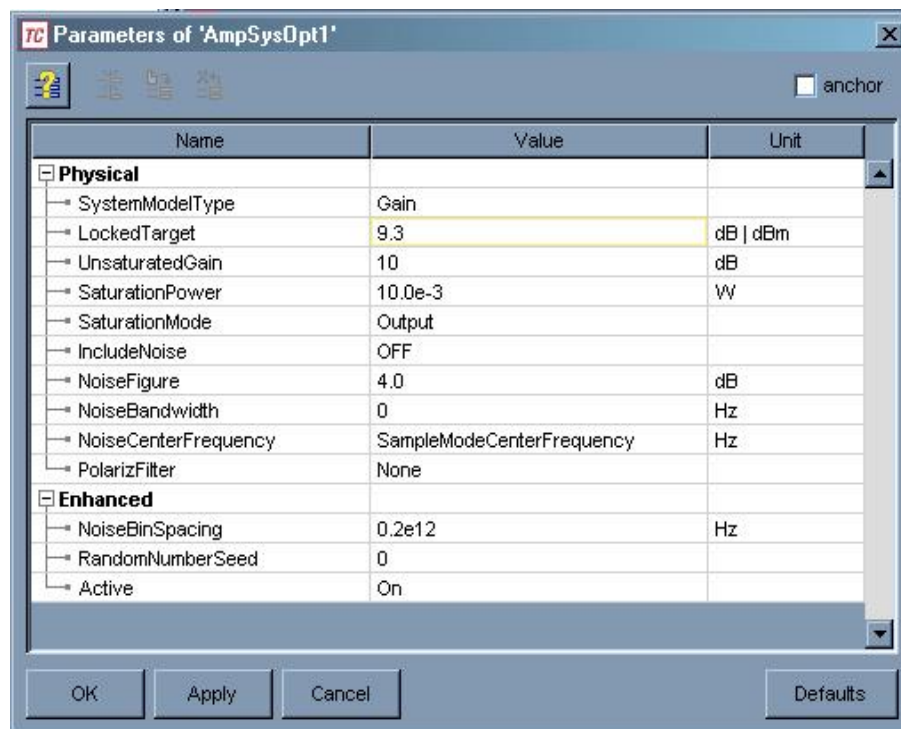


Figure 4.8. Parameters of Ideal Amplifier

4.9 Results

In the simulation, the total output wave is the summation of each interference signal. Recall the equations (4.7), (4.10).

$$P_{total}(t) = \frac{K \{1 + \nu \cos[\phi_s + \phi_e \cos(\omega_m t)]\}}{1 - AK' \{1 + \nu \cos[\phi_s + \phi_e \cos(\omega_m t)]\}}, \text{ and} \quad (4.7)$$

$$[\phi_s + \phi_e \cos(\omega_m t)] = 2n\pi, \quad n=0, 1, 2, \dots \quad (4.10)$$

As it is said before, in order to achieve sharp pulses, frequency of the phase modulator must be selected properly: $\omega_m \tau = 2n\pi$ (τ : total round trip time). In the simulation, Sagnac loop delay τ_s is $1,8 \mu\text{s}$ and feedback delay is $0,3 \mu\text{s}$. So $\tau = 2,1 \mu\text{s}$ and $f_m = \omega_m / 2\pi = 4.76 \cdot 10^5 \text{ Hz}$.

First, the simulation is run for nonrotation case ($\phi_s = 0$). This means that phase shifters are set to zero. Here, equation 4.10 is satisfied only when $n = 0$. In this case, the peak positions of the output pulse are determined by

$$\omega_m t_0 = \frac{2i+1}{2} \pi, \quad i = 0, 1, 2, \dots \quad (4.11)$$

Here t_0 represents the peak positions corresponding to the nonrotation case and i denotes the peak number of the output pulse in the time axis. Peak positions are not affected by the phase modulation depth ϕ_e when there is no rotation. Figure 4.9 shows the output of the simulation when $\phi_s = 0$, $\phi_e = 1.24 \pi \text{ rad}$.

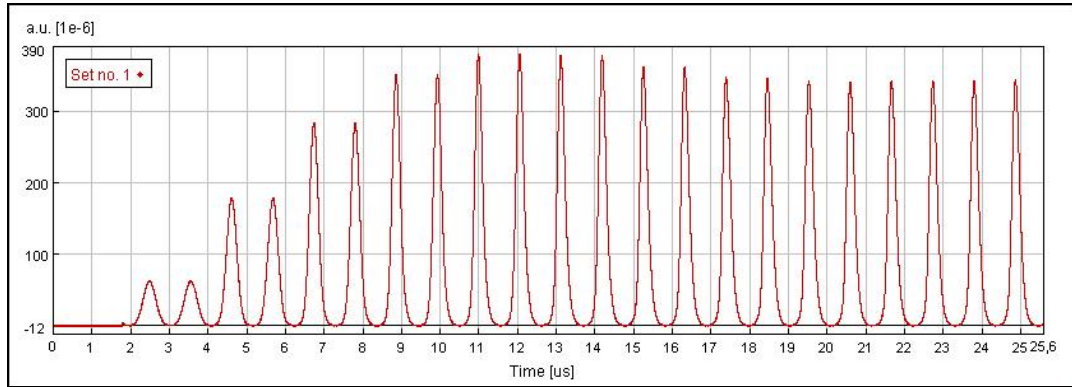


Figure 4.9. Output signal for $\phi_s = 0$, $\phi_e = 1.24 \pi$ rad.

As it is seen that the peak positions are not clear at early microseconds. So, in our studies, the later peaks are used for analyzing data.

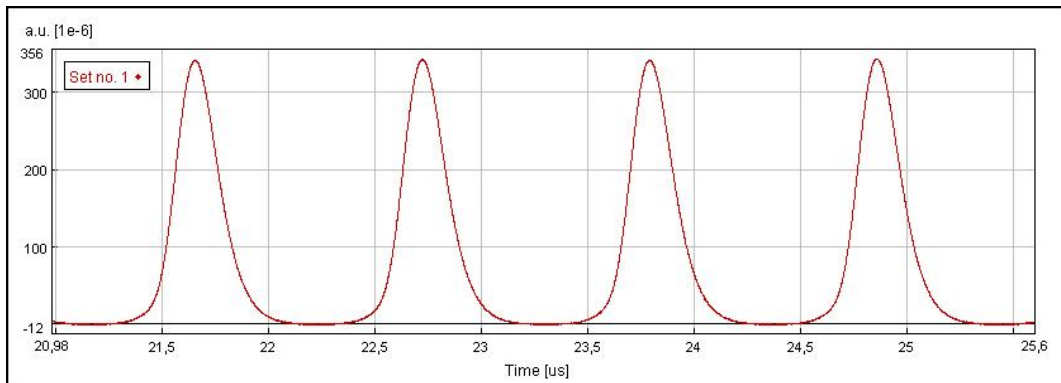


Figure 4.10. Later output pulses for $\phi_s = 0$, $\phi_e = 1.24 \pi$ rad.

In the Figure 4.10, the peak number of the first peak is $i = 20$. Using the equation (4.11), the value for t_0 can be calculated as $21.539 \mu\text{s}$. Here this value is $21.655 \mu\text{s}$. Calculations are not affected by this shift because all peaks are equally shifted.

Figure 4.11 shows the output of the simulation when $\phi_s = 0$, $\phi_e = 1.85 \pi$ rad. When Figure 4.9 and figure 4.11 are compared, the relation between ϕ_e and sharpness is obviously seen.

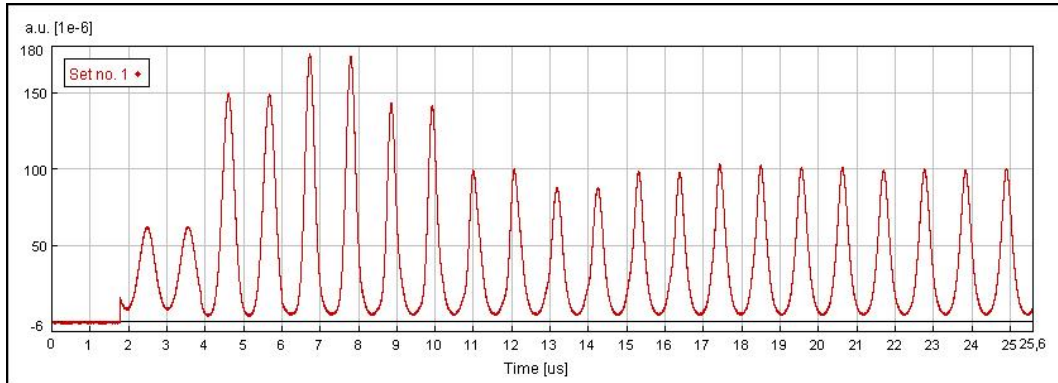


Figure 4.11. Output signal for $\phi_s = 0$, $\phi_e = 1.85 \pi$ rad.

The shape of the pulse depends on two variables: gain of the amplifier and modulation depth ϕ_e . The sharpness of the pulse can be adjusted by both the gain and ϕ_e . If the gain is increased, the pulse can be sharpened.

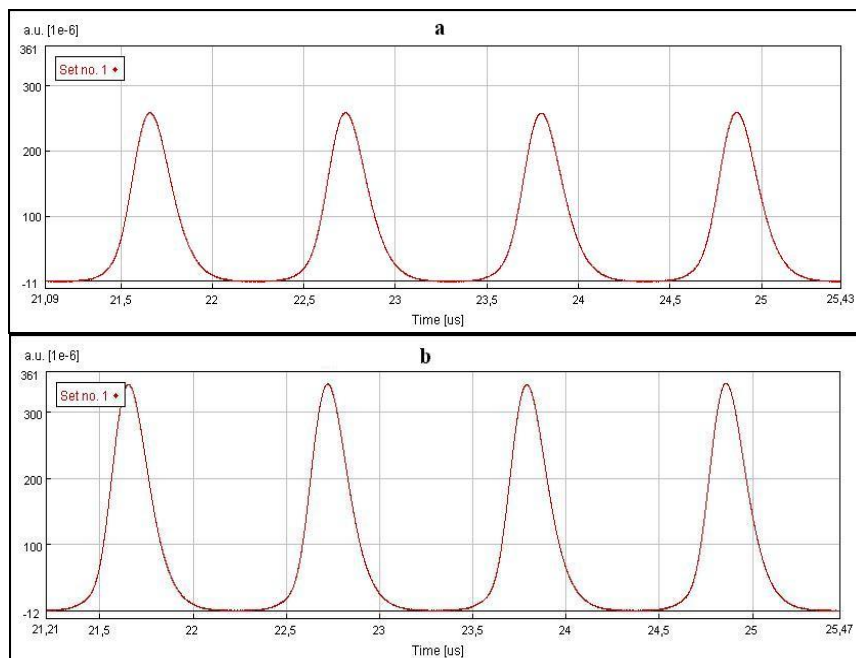


Figure 4.12. Comparison between two gain values (a) 8 dB and (b) 9.3 dB for $\phi_e = 1.24 \pi$ rad.

On the other hand, when rotation occurs (i.e., $\phi_s \neq 0$), the peak positions are influenced by the Sagnac phase shift and can be determined by

$$\omega_m t_r = \arccos\left(-\frac{\phi_s}{\phi_e}\right) + 2i\pi, \quad i = 0, 1, 2, \dots \quad (4.12)$$

where t_r denotes the peak positions when rotation occurs and i has the same meaning as in equation (4.11). We can see that the peak positions shift if rotation occurs, and shift of the peaks is just equal to $\Delta t = t_r - t_0$. Therefore, the peak positions are influenced by only the Sagnac phase shift if rotation occurs and if the phase modulation depth is fixed (Figure 4.13). The rotation rate can be determined by the detection of the peak shift Δt of the output pulse. Here, it has to be mentioned that

for $i = 0, 2, 4, \dots$; $\Delta t < 0$ and for $i = 1, 3, 5, \dots$; $\Delta t > 0$.

The Sagnac phase shift ϕ_s is

$$\phi_s = \frac{4\pi RL}{\lambda_0 c} \Omega \quad (4.13)$$

and using equations (4.10), (4.12), rotation rate can be derived as for $i = 0, 2, 4, \dots$ in equation (4.11)

$$\begin{aligned} \Omega &= -\frac{\lambda_0 c}{4\pi RL} \phi_e \cos(\omega_m t_0 + \omega_m \Delta t) \\ &= \frac{\lambda_0 c}{4\pi RL} \phi_e \sin(\omega_m \Delta t) \end{aligned} \quad (4.14)$$

The simulation program is run for different ϕ_e and ϕ_s values. Outputs of the simulations are given below.

For $\phi_e = 1.85 \pi$ rad;

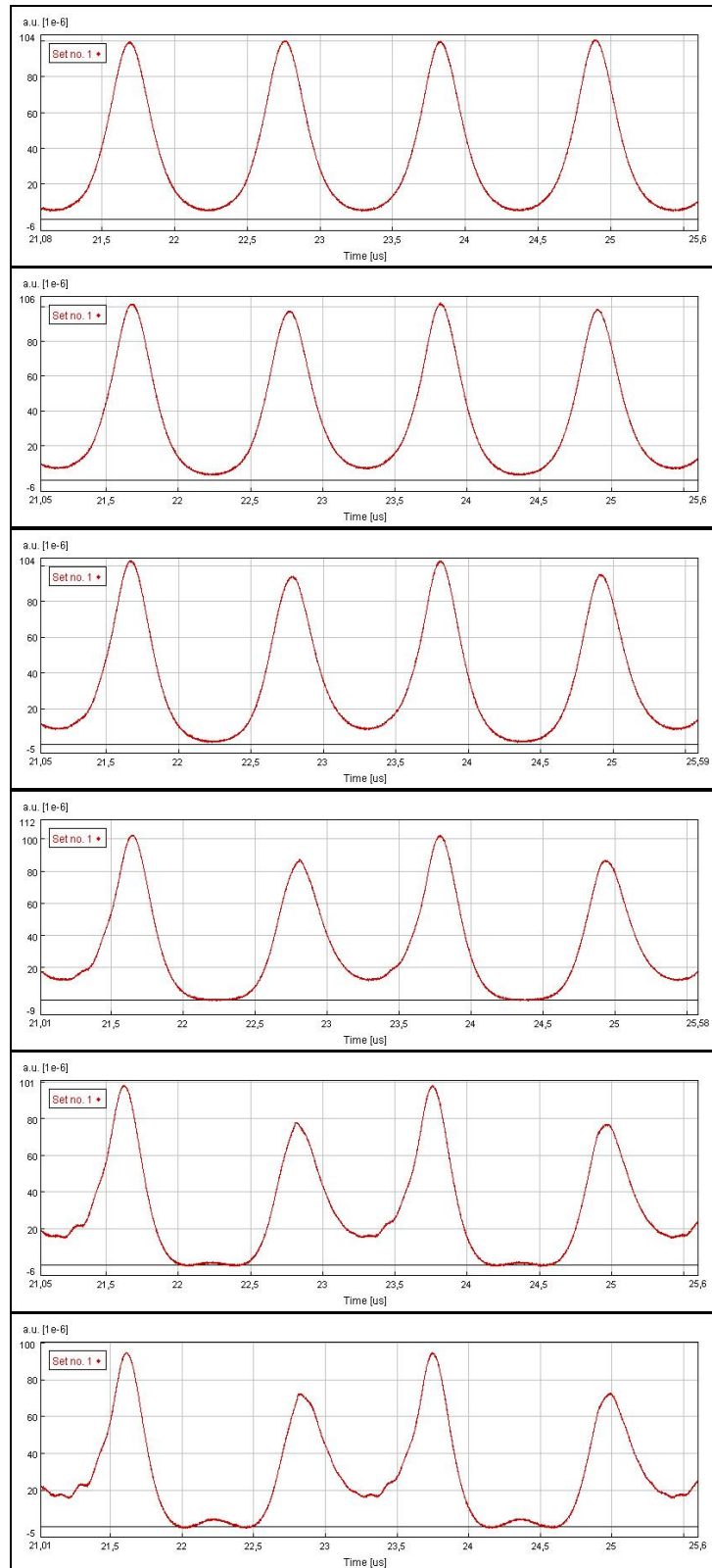


Figure 4.13. Results for $\phi_e = 1.85 \pi$ rad

For $\phi_e = 1.24 \pi \text{ rad}$;

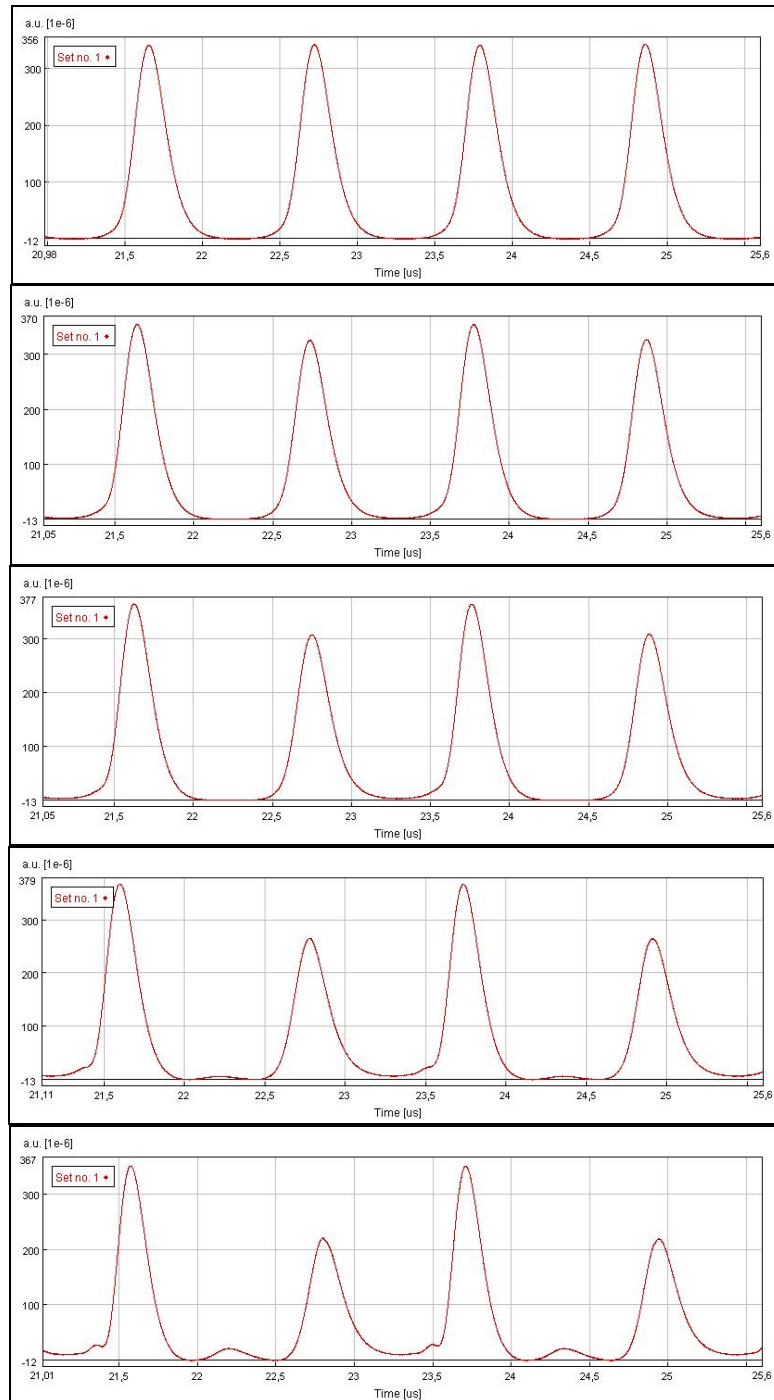


Figure 4.14. Results for $\phi_e = 1.24 \pi \text{ rad}$

Calculations of time shifts ($\Delta t = t_r - t_0$) and rotation rates (eqn.4.14):

For $\phi_e = 1.85 \pi$ rad;

$$\begin{aligned} \phi_s = 10^\circ &\Rightarrow \Delta t = 0.010 \mu\text{s} \Rightarrow \Omega = 12,74 \text{ }^\circ/\text{s} \\ \phi_s = 20^\circ &\Rightarrow \Delta t = 0.020 \mu\text{s} \Rightarrow \Omega = 25,47 \text{ }^\circ/\text{s} \\ \phi_s = 40^\circ &\Rightarrow \Delta t = 0,040 \mu\text{s} \Rightarrow \Omega = 50,85 \text{ }^\circ/\text{s} \\ \phi_s = 60^\circ &\Rightarrow \Delta t = 0.060 \mu\text{s} \Rightarrow \Omega = 76,06 \text{ }^\circ/\text{s} \\ \phi_s = 70^\circ &\Rightarrow \Delta t = 0,070 \mu\text{s} \Rightarrow \Omega = 88,56 \text{ }^\circ/\text{s} \end{aligned}$$

For $\phi_e = 1.24 \pi$ rad;

$$\begin{aligned} \phi_s = 10^\circ &\Rightarrow \Delta t = 0.015 \mu\text{s} \Rightarrow \Omega = 12,81 \text{ }^\circ/\text{s} \\ \phi_s = 20^\circ &\Rightarrow \Delta t = 0.030 \mu\text{s} \Rightarrow \Omega = 25,59 \text{ }^\circ/\text{s} \\ \phi_s = 40^\circ &\Rightarrow \Delta t = 0.060 \mu\text{s} \Rightarrow \Omega = 50,98 \text{ }^\circ/\text{s} \\ \phi_s = 60^\circ &\Rightarrow \Delta t = 0.090 \mu\text{s} \Rightarrow \Omega = 75,96 \text{ }^\circ/\text{s} \end{aligned}$$

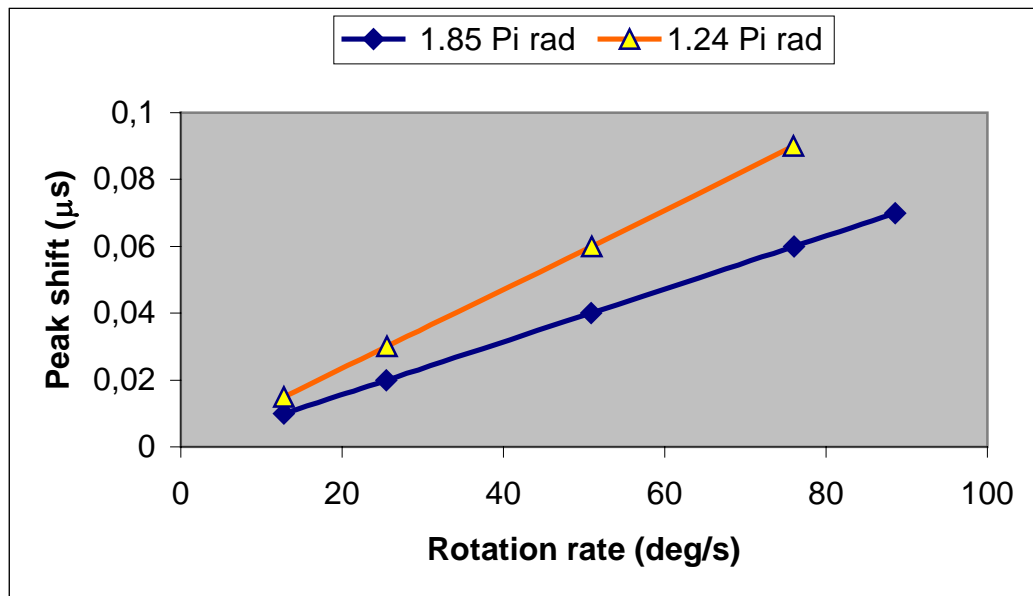


Figure 4.15. Time shift of the output peak as the function of rotation rate with different phase modulation $\phi_e = 1.85 \pi$ rad, $\phi_e = 1.24 \pi$ rad.

For all above calculations ϕ_s was positive but ϕ_s can also take negative values which means opposite rotation direction. Figure 4.16 shows the results for negative rotation when $\phi_s = -20^\circ$, $\phi_e = 1.24 \pi$ rad.

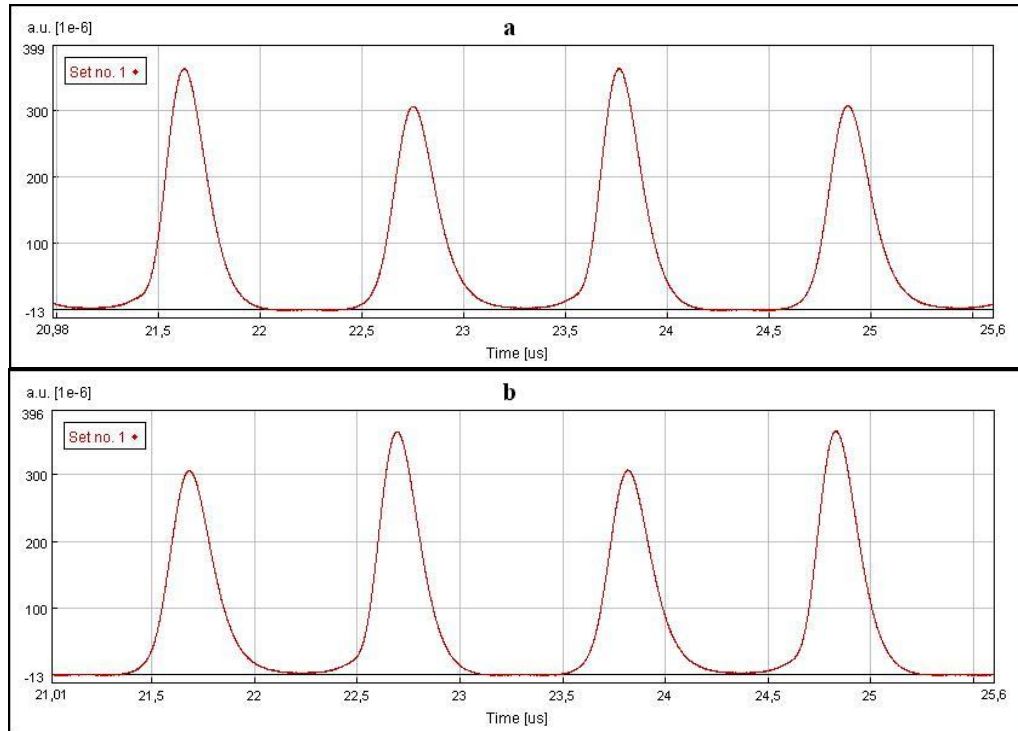


Figure 4.16. Comparison between (a) positive rotation $\phi_s = 20^\circ$ and (b) negative rotation $\phi_s = -20^\circ$, when $\phi_e = 1.24 \pi$ rad.

As it is seen from the Figure 4.16, the peak positions are shifted through the opposite direction comparing the positions at $\phi_s = -20^\circ$ with the positions at $\phi_s = +20^\circ$. That means, using this configuration not only the rotation rates can be calculated but also the rotation way can be determined.

CHAPTER 5

CONCLUSION

In this work, a novel interferometric fiber optic gyroscope that is based on multiple utilizations of the Sagnac loop by amplified optical feedback (FE_FOG) has been proposed and simulated. A software, VPItransmissionMakerTM, developed by VPIsystems, was used.

In FE_FOG, low coherence light sources (SLD) are used. There is no such kind of source in VPItransmissionMakerTM so a laser continuous wave (LaserCW) was used in simulation. Amplification of a weak feedback gyroscope signal was performed by EDFA.

The output of this gyroscope is in pulse state if the modulation frequency of the phase modulator matches the total round trip. The round-trip time was calculated and proper modulation frequency was selected.

The resolution of the rotation measurement depends on the sharpness of the output pulse. The sharpness of the output pulse was adjusted with the gain of amplifier and the phase modulation depth. It is seen that, increasing the gain of the amplifier improves the sharpness of the output pulse.

The positions of the output pulses, which is important to measure the rotation rate, were determined for several phase modulation depth and Sagnac phase shift values. Sagnac phase shift induces a shift of the output pulse in time axis. If rotation rate increase, the peak shift also increase.

Getting time shift values for different Sagnac phase shifts from the software, a graph, peak shift versus rotation rate, was plotted. These calculations were done for two different values of phase modulation depth. It can be seen that, using smaller phase modulation depth increases the resolution. For smaller phase modulation depth, the gain of amplifier was adjusted to get sharp pulses. On the other hand, increasing the phase modulation depth provide a large dynamic range.

REFERENCES

- [1] Loukianov, D., Rodloff, R., Sorg, H. and Stieler, B., "Introduction", *Optical Gyros and Their Applications_RTO, AGARDograph 339*, p.1-1, 1999.
- [2] Rodloff, R., "Physical Background and Technical Realization", *Optical Gyros and Their Applications_RTO, AGARDograph 339*, p.2-1, 1999.
- [3] Marison, J.B. and Thomton, S.T., *Classical Dynamics of Particals and Systems*, 3rd ed. Harcourt Brace, Jovanovich, 1988.
- [4] Griffiths, D.J., *Introduction to Electrodynamics*, 2nd ed. Prentice Hall, Engiewood Cliffs, New Jersey, 1989.
- [5] Hecht, E. and Zajac, A., *Optics*, Addison Wesley, 1988.
- [6] Lefevre, H., *The Fiber-Optic Gyroscope*, Artech House, Norwood, Massachusetts, 1993.
- [7] Lefèvre, H.C., "Application of the Sagnac Effect in the Interferometric Fiber-Optic Gyroscope", *Optical Gyros and Their Application_RTO, AGARDograph 339*, p.7-1, 1999.
- [8] Blake, J., *Fiber Optic Gyroscopes in Optical Sensor Technology*, Vol.2, Grattan K.T.V. and Meggitt B.T. Eds., Chapman and Hall, London, 1988.
- [9] Steven, J.S. (Honeywell Technology Center), *Lecture Notes; Intro the FOG: A Course on Fiber-Optic Gyroscopes*, Ankara Turkey, 2000.

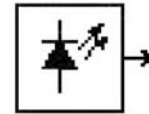
- [10] Bergh, R., Lefevre H.C., Shaw H. J., “An Overview of Fiber-Optic Gyroscopes”, *Journal of Lightwave Technology*, vol.2, no.2, April 1984.
- [11] Lefevre, H., “Fundamentals of The Interferometric FOG”, *Photonetics, SPIE* vol. 2837, p2-15.
- [12] Pollock, C. R., *Fundamentals of Optoelectronics*, Irwin, 1995.
- [13] Burns, W. K., Chen C.L., R. P. Moeller, “Fiber Optic Gyroscopes with broadband sources”, *Journal of Lightwave Technology*, vol. 1, no. 1, pp. 98-105, March 1983.
- [14] Wagener, J. L., Dignonnet M. J. F., and Shaw H. J., “ A High Stability Fiber Amplifier Source for the Fiber Optic Gyroscope”, *Journal of Lightwave Technology*, vol.15, no.9, September 1997.
- [15] Kumagai, T., et all. . : “Optical Gyrocompass Gsing A Fiber Optic Gyroscope with High Resolution” *Proceeding of 9th Meeting on Lightwave Sensing Technology, L S T 9-16-5*, pp.125, 1992.
- [16] Wang, L. A, Su C.D., “Modeling of a Double-Pass Backward Er-Doped Superfluorescent Fiber Source for Fiber Optic Gyroscope Applications”, *Journal of Lightwave Technology*, vol.17, no.11, November 1999.
- [17] Wanser, K.H., “Fundamental Phase Noise Limit in Optic Fibers due to Temperature Fluctuations” *Electronic Letters.*, 28, 53, 1992.
- [18] Burns, W.K., Moeller R.P., Dandridge A, “Excess Noise in Fiber Gyroscope Sources”, *IEEE Photonics Tech. Lett.* 2, 606, 1990.

- [19] Shi, C. X., Yuhara T., Lizuka H., and Kajioka H., “New Interferometric Fiber Optic Gyroscope with Amplified Optical Feedback”, *Applied Optics*, vol.35, no. 3, 1996.
- [20] VPItransmissionMaker™ Manuals
- [21] http://www.vpiphotonics.com/pda_design.html
- [22] Shupe, D.M., “Thermally Induced Nonreciprocity in Fiber-Optic Interferometer”, *Applied Optics*, vol. 9, p. 654-655, 1980.
- [23] Bergh, R. A., “Source Statistics and the Kerr Effect in Fiber-Optic Gyroscopes”, *Optics Letters*, vol. 7, p. 563-565, 1982.
- [24] Meyer, R. E., S. Ezekiel, D. W. Stowe, and V. J. Tekippe, “Passive Fiber-Optic Ring Resonator Resonator for Rotation Sensing”, *Opt. Lett.*, vol. 8, 1983, pp. 644–6.
- [25] Carrol, R., and Potter, J. E., “Backscatter and the Resonant Fiber-Optic Gyro Scale Factor”, *IEEE J. Lightwave Technol.*, vol.LT-7, 1989, pp. 1895–900.

APPENDIX A

Modules Used in The Simulation

A.1 Laser CW



The module produces a continuous wave (CW) optical signal. It can be used as a pump source.

Outputs

output = continuous wave optical signal
(signal type: *Optical Blocks*, *Optical Samples*)

Physical Parameters

Name and Description	Symbol	Unit	Type	Volatile	Value Range	Default Value
EmissionFrequency Laser emission frequency	f_c	Hz	real	yes]0,∞[2.9979e8/980e-9 #conversion from wavelength
SampleRate Sample rate of the system	f_s	Hz	real	no]0,∞[SampleRateDefault
AveragePower Average output power	P_{ave}	W	real	yes	[0,∞[1.0e3
Linewidth Linewidth of the laser	Δf	Hz	real	yes	[0,∞[10e6
Azimuth Azimuth angle of the output polarization	η	deg	real	yes]-90,90]	0

Ellipticity Ellipticity angle of the output polarization	ε	deg	real	yes	[-45,45]	0
InitialPhase Initial phase	ϕ_c	deg	real	no]- ∞ , ∞ [0

Enhanced Simulation Parameters

Name and Description	Symbol	Unit	Type	Volatile	Value Range	Default Value
RandomNumberSeed Lookup index for noise generation; a value of zero implies an automatic, unique seed.	___	___	int	no	[0,10000]	0
NoiseBandwidth Bandwidth in which Noise Bins are created.	___	Hz	real	no	[0, ∞ [0
NoiseDynamic Maximum allowed ratio of noise "coloredness" within one single bin	___	dB	real	no]- ∞ , ∞ [3.0
NoiseThreshold Noise threshold for adaption of Noise Bins.	___	dB	real	no]- ∞ , ∞ [-100
OutputDataType Defines if to produce signal blocks or statistical signals.	___	___	enum	no	BLOCKS, PARAMETRIZED	BLOCKS
Active Defines if the module is active or not.	___	___	enum	yes	ON, OFF	ON

Description

The module produces a time dependent field $E_b(t)$ Parameterized Signal, which is normalized to the user-specified power P_{ave} (parameter **AveragePower**). The emission frequency of the cw-laser is defined by the parameter **EmissionFrequency**.

The laser model (see Figure A.1) contains a Gaussian white noise source with a variance of $2\pi\Delta f$ corresponding to the optical laser **Linewidth** Δf .

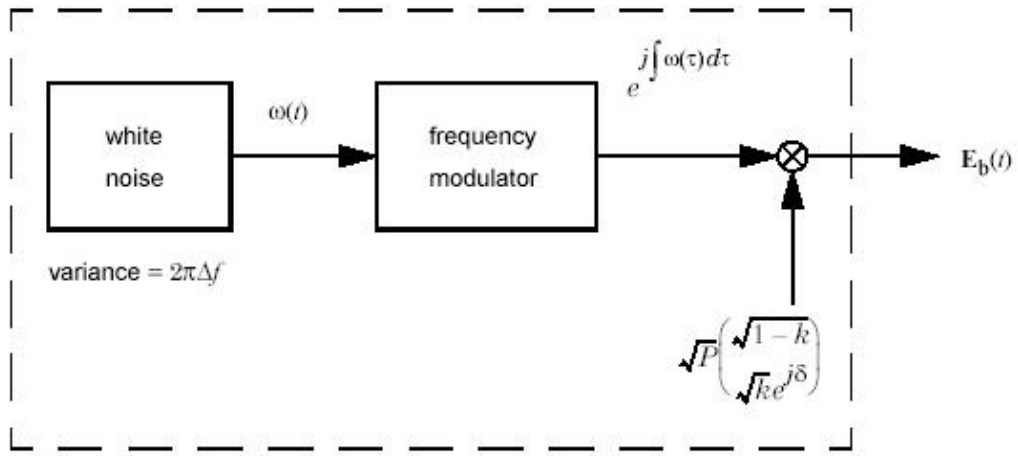


Figure A.1. Schematic of the modeled DFB CW laser

The output is multiplied with a complex vector considering the state of polarization (SOP), to obtain the X and Y polarization components. The baseband signal of the optical output cw-wave is therefore determined by

$$E_b(t) = \sqrt{P} \begin{bmatrix} \sqrt{1-k} \\ \sqrt{k} e^{j\delta} \end{bmatrix} \cdot \exp[j\int \omega(\tau) d\tau] \quad (\text{A.1})$$

The SOP is given by the power splitting parameter k ($0 \leq k \leq 1$) and an additional phase δ . The relations of k and δ with the **Azimuth** η and the **Ellipticity** ε are given by

$$\begin{aligned}\tan(2\eta) &= 2 \frac{\sqrt{k(1-k)} \cdot \cos \delta}{1-2k} \\ \sin(2\varepsilon) &= 2\sqrt{k(1-k)} \cdot \sin \delta\end{aligned}\tag{A.2}$$

With the parameter **InitialPhase** ϕ_c , the user can determine the initial phase of the optical carrier. The parameter **RandomNumberSeed** specifies an index of a lookup table for the generation of the laser phase noise. A value of zero produces a unique seed to start the noise generator. This assures that each noise field generated in the simulation is not correlated to all other noise fields, since a unique seed is used for each noise generation. Note that for user-specified seed values, correlation between different noise processes can occur.

The parameter **OutputDataType** defines if the module produces optical BLOCKS, SAMPLES or PARAMETRIZED signals as output data.

Signal Representation: Individual Samples

Individual Sample Mode is supported by this module.

Boundary Conditions

Both periodic and aperiodic boundary conditions are supported.

Reinitialization Behavior

Multiple Runs:

In the first run, a unique seed is occupied by each module if the start seed value was chosen to zero. On consecutive runs, the individual random sequence of each

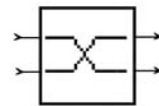
module is continued (aperiodic boundary conditions) or repeated (periodic boundary conditions).

Restart of Simulation:

If the simulation is restarted, the same seed values from the lookup table are used for noise generation. Note that topology changes may change the specific seed value used by a module.

Module Deactivation:

If parameter **Active** is OFF, the laser is switched off and no output signal is generated.



A.2 X Coupler

The module models an optical coupler for combining or splitting of optical signals. It can also be used as a physical signal splitter for signal check.

Inputs

input1 = optical signal
(signal type: *Optical Blocks, Optical Samples*)

input2 = optical signal
(signal type: *Optical Blocks, Optical Samples*)

Outputs

output1 = optical signal
(signal type: *Optical Blocks, Optical Samples*)
output2 = optical signal
(signal type: *Optical Blocks, Optical Samples*)

Physical Parameters

Name and Description	Symbol	Unit	Type	Volatile	Value Range	Default Value
CoupleFactor Specifies the cross_coupling coefficient, from port 1 to port 2.	α	—	real	yes	[0,1]	0.5

In our simulation, same parameter values are used.

Signal Representation: Samples

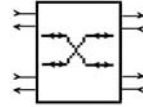
The cross coupler is defined by its transmission matrix (A.3)

$$\begin{pmatrix} \mathbf{E}_{1, \text{out}} \\ \mathbf{E}_{2, \text{out}} \end{pmatrix} = \begin{pmatrix} \sqrt{1-\alpha} & j\sqrt{\alpha} \\ j\sqrt{\alpha} & \sqrt{1-\alpha} \end{pmatrix} \cdot \begin{pmatrix} \mathbf{E}_{1, \text{in}} \\ \mathbf{E}_{2, \text{in}} \end{pmatrix}, \quad (\text{A.4})$$

with the **CoupleFactor** α . $E_{1,\text{in}}$ and $E_{2,\text{in}}$ are the input electrical fields and $E_{1,\text{out}}$ and $E_{2,\text{out}}$ are the output fields at the ports 1 and 2 of the coupler, respectively.

Boundary Conditions

Both, periodic and aperiodic boundary conditions are supported.



A.3 X Coupler Bidirectional

The module acts as a bidirectional X Coupler. It is implemented as two independent X Couplers, one for forward and one for backward direction.

Inputs

in1Forward = optical signal

(signal type: *Optical Blocks*, *Optical Samples*)

in2Forward = optical signal

(signal type: *Optical Blocks*, *Optical Samples*)

in1Backward = optical signal

(signal type: *Optical Blocks*, *Optical Samples*)

in2Backward = optical signal

(signal type: *Optical Blocks*, *Optical Samples*)

Outputs

out1Backward = optical signal

(signal type: *Optical Blocks*, *Optical Samples*)

out1Forward = optical signal

(signal type: *Optical Blocks*, *Optical Samples*)

out2Backward = optical signal

(signal type: *Optical Blocks*, *Optical Samples*)

out2Forward = optical signal

(signal type: *Optical Blocks*, *Optical Samples*)

Physical Parameters

Name and Description	Symbol	Unit	Type	Volatile	Value Range	Default Value
CoupleFactor Specifies the cross_coupling coefficient	α	—	real	yes	[0,1]	0.5

Description

The module acts as a bidirectional X Coupler. It is implemented as a Galaxy consisting of two independent X Couplers as depicted in Figure A.2. The parameter **CoupleFactor** specifies the coupling strength of the two Couplers. No interaction between forward and backward propagating signals is considered.

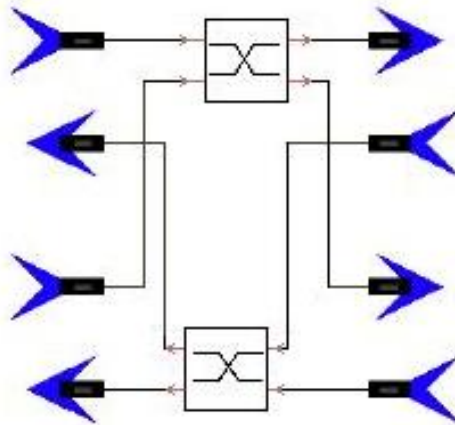
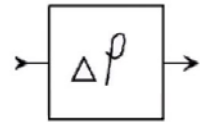


Figure A.2. Implementation of the XCouplerBi Galaxy



A.4 Phase Shift

The module adds a time-independent phase advance to the optical input signal.

Inputs

input = optical signal
(signal type: *Optical Blocks*, *Optical Samples*)

Outputs

output = optical signal
(signal type: *Optical Blocks*, *Optical Samples*)

Physical Parameters

Name and Description	Symbol	Unit	Type	Volatile	Value Range	Default Value
PhaseShift Phase shift to apply	$\Delta\phi$	deg	real	yes	$]-\infty, \infty[$	0

Enhanced Simulation Parameters

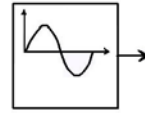
Name and Description	Symbol	Unit	Type	Volatile	Value Range	Default Value
Active Defines if the module is active or not.	___	___	enum	yes	ON, OFF	ON

Description

The module applies a phase shift of $\Delta\phi$, specified by the parameter **PhaseShift** to the signal. All sampled values are multiplied by $\exp(j\Delta\phi)$.

Signal Representation: Individual Samples

Each sample is advanced by the same optical phase.



A.5 Sine Generator (Electrical)

This module generates an electrical sine waveform superimposed on a constant bias.

Outputs

output = Output of electrical signal
(signal type: *Electrical Blocks*, *Electrical Samples*)

Physical Parameters

Name and Description	Symbol	Unit	Type	Volatile	Value Range	Default Value
SampleRate Sample rate of the output signal	—	Hz	real	no	$]0, \infty[^a$	SampleRateDefault
Amplitude Zero-to-peak amplitude of the output signal.	E_0	a.u.	real	yes	$[0, \infty[^a$	1.0
Frequency Frequency of output signal.	f	Hz	real	yes	$[0, \text{sample rate}/2[^a$	$1e8$
Phase Initial phase of output signal.	φ	deg	real	yes	$[0, \infty[^a$	0.0
Bias DC offset of output signal.	E_{bias}	a.u.	real	yes	$] -\infty, \infty[^a$	0.0

Enhanced Simulation Parameters

Name and Description	Symbol	Unit	Type	Volatile	Value Range	Default Value
OutputDataType Defines type of output: Sample Mode or Block Mode..	___	___	enum	no	SAMPLES, BLOCKS	BLOCKS
Active Defines if the module is active or not.	___	___	enum	yes	ON, OFF	ON

Description

This module can be used to generate a sine signal of arbitrary amplitude and initial phase, as adjusted with **Amplitude and Phase**, respectively. The frequency may be chosen from zero Hz (DC) up to a value lower than half the sample rate. A DC Offset may be applied to the signal using **Bias**.

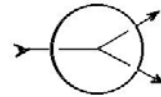
The electrical output signal of the module is determined by

$$E_{\text{out}} = E_{\text{bias}} + E_0 \sin(2\pi ft + \varphi) \quad (\text{A.5})$$

where E_{bias} denotes the **Bias**, f the **Frequency** and φ the initial **Phase**.

Signal Representation: Individual Samples

If parameter **OutputDataType** is set to Samples, the module produces an output signal in *Sample Mode*, at a sample rate equal to the global variable **SampleModeBandwidth**.



A.6 Multiple Output Connector (Fork)

Copy input particles to each output.

Inputs

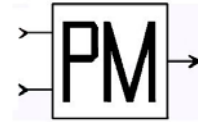
input = Input
(signal type: *anytype*)

Outputs

output = Output
(signal type: *anytype*)

Description

This star is generally used to connect a single output port to multiple input ports. It will be automatically inserted when multiple inputs are connected to the same output using the graphical interface, or when the "nodeconnect" command is used in the interpreter. However, there are times when automatically inserted Fork stars are not desirable. For instance, when there is a delay on one of the arcs, then the Fork must be inserted by the user explicitly to avoid ambiguity about the location of the delay. Also, when multi-portholes are used, auto-forking can cause problems. In this situation, one may get, for example, two outputs and several inputs on the same net. There is currently no way to automatically decipher what the user intends. Hence, the Fork star should be inserted explicitly.



A.7 Modulator Phase

The module simulates an ideal phase modulator (PM).

Inputs

carrier = optical carrier

(signal type: *Optical Blocks, Optical Samples*)

data = electrical modulation signal; must be within the range [0,1]

(signal type: *Electrical Blocks, Electrical Samples*)

Outputs

output = modulated optical signal

(signal type: *Optical Blocks, Optical Samples*)

Physical Parameters

Name and Description	Symbol	Unit	Type	Volatile	Value Range	Default Value
PhaseDeviation Phase difference between marks and spaces	$\Delta\phi$	deg	real	yes	$]-\infty, \infty[$	180

Enhanced Simulation Parameters

Name and Description	Symbol	Unit	Type	Volatile	Value Range	Default Value
Active Defines if the module is active or not.	—	—	enum	no	ON, OFF	ON

Description

The output signal $E_{\text{out}}(t)$ is given by

$$E_{\text{out}}(t) = E_{\text{in}}(t) \cdot \exp[j\Delta\phi \text{ data}(t)], \quad (\text{A.6})$$

where $E_{\text{in}}(t)$ denotes the input optical signal, $\text{data}(t)$ represents the electrical modulation signal, and $\Delta\phi$ denotes the phase deviation specified by parameter

PhaseDeviation.

The optical power is not affected by the phase modulator.

If the electrical and optical input signals have different sample rates, the signal that has the lower sample rate is upsampled.

Arbitrary polarization state is allowed for the input optical signal. The output polarization is the same as the input one.

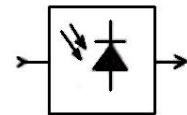
Signal Representation: Individual Samples

Each sample is processed in the time domain according to (A.6).

Reinitialization Behavior

Module Deactivation:

If parameter **Active** is OFF, the optical input signals will be passed through the module without any changes.



A.8 Photodiode PIN

The module acts as a PIN photodiode with additive Gaussian white noise sources.

Inputs

input = optical signal
(signal type: *Optical Blocks, Optical Samples*)

Outputs

output = electrical signal
(signal type: *Electrical Blocks, Electrical Samples*)

Physical Parameters

Name and Description	Symbol	Unit	Type	Volatile	Value Range	Default Value
Responsivity Responsivity of the photodiode.	r	A/W	real	yes	[0,2]	1.0
ThermalNoise Thermal noise of additional preamplifier/load resistor.	N_{th}	$\frac{A}{\sqrt{Hz}}$	real	yes	[0,100- 10 ⁻¹²]	10.0e-12
DarkCurrent Dark current.	i_d	A	real	yes	[0,10.10 ⁻⁶]	0.0
ShotNoise Switch shot noise ON or OFF .	—	—	enum	no	ON, OFF	ON

Enhanced Simulation Parameters

Name and Description	Symbol	Unit	Type	Volatile	Value Range	Default Value
RandomNumberSeed Lookup index for noise generation; a value of zero implies an automatic, unique seed.	___	___	int	no	[0,10000]	0

Description

The module converts the incident optical field into an electrical signal. Since at the input, several separated sampled optical bands may be present, all optical bands are joined to one sampled optical band. Noise Bins falling within the combined sampled band's bandwidth are added after conversion to random Gaussian optical fields. The combined optical field $E(t)$ is then converted into an optical power $P_s(t)$ by taking its modulus squared, and converting to an electrical signal as described below.

For modeling a PIN photodetector, the process of converting the optical intensity into an electrical current is described by

$$i(t) = i_s(t) + n_{sh}(t) + n_{th}(t) + i_d \quad (\text{A.7})$$

In this equation:

- With the **Responsivity** r the output signal current $i_s(t)$ is directly related to the absorbed optical power $P_s(t)$ by $i_s(t) = r \cdot P_s(t)$.

n_{sh} denotes the generated **ShotNoise** current with the one-sided spectral noise density N_{sh} in A/\sqrt{Hz} . The spectral density is determined by

$$N_{sh} = 2q \cdot (i_s + i_d), \quad (\text{A.8})$$

if **ShotNoise** is switched ON.

- n_{th} represents the **ThermalNoise** caused by the (usually high) photodetector's internal resistance. The associated one-sided spectral noise density N_{th} has to be specified by the user in A/\sqrt{Hz} .
- i_d denotes the PIN **DarkCurrent**.

This is illustrated in Figure A.3.

The statistically independent noise currents, n_{sh} and n_{th} , are created with the aid of the noise generator. The seed value for the noise generator is specified by the parameter **RandomNumberSeed**. If a default value of zero is chosen the used seed value is unique in the simulation. This means that the noise sequence is uncorrelated to each other noise sequence used in the simulation.

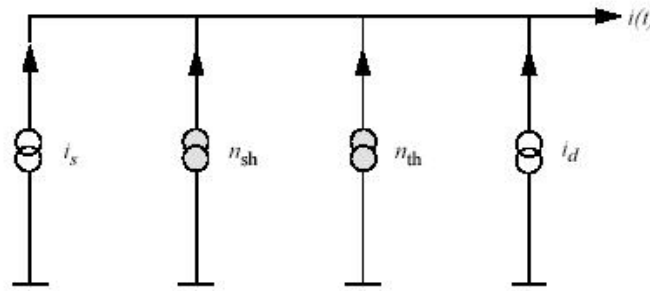


Figure A.3. Noise equivalent diagram of a PIN-Direct-Receiver

Signal Representation: Individual Samples

The Sample Mode is supported.

Boundary Conditions

Both periodic and aperiodic boundary conditions are supported.

Reinitialization Behavior

Multiple Runs:

In the first run, a unique seed is occupied if the parameter **RandomNumberSeed** is chosen to zero. On consecutive runs, the individual random sequence of the module using the noise generator is continued.

Restart of Simulation:

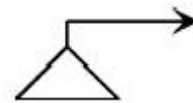
If the simulation is restarted, the same seed value from the lookup table is used for noise generation. Note that topology changes may change the specific seed value used by a module.

Module Deactivation:

Currently not available.

Error Indications and Warnings

A warning message occurs if only Noise Bins or Parameterized Signals are available as an input signal.



A.9 Null Source

The module represents a null source for signals of any type. This module is required to terminate all unused inputs.

Outputs

output = optical or electrical signal

(signal type: *Optical Blocks, Optical Samples,*
Electrical Blocks, Electrical Samples)

Enhanced Simulation Parameters

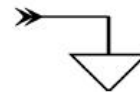
Name and Description	Symbol	Unit	Type	Volatile	Value Range	Default Value
<p>OutputSignal Defines if to produce optical or electrical kind of output data.</p>	—	—	enum	no	Electrical, Optical	Optical
<p>OutputDataType Defines whether to generate Block Mode or Sample Mode signal.</p>	—	—	enum	no	Samples, Blocks	Blocks

In our simulation, **OutputSignal** is ‘Optical’ and **OutputDataType** is ‘Samples’.

Description

The module is typically used to provide subsequent modules with a null input. The parameter **OutputSignal** chooses the output data type. Depending on the input type of the connected module, the type has to be chosen properly to prevent data type mismatching to the input of the following module. The parameter **OutputDataType** chooses the data type of the signal. It can be block mode or sample mode.

A.10 Ground



The *Ground* module discards input signals. This module is required to terminate unused output ports of all modules. The Design Assistant *AutoGrounds* will do this automatically.

Inputs

input (multiple) = optical or electrical signal
(signal type: *anytype*)

Description

To discard signals of any type which are of no further interest, this module can be applied as the termination (data sink).

Signal Representation: Individual Samples

The sample mode is supported by this module.

Boundary Conditions

Both periodic and aperiodic boundary conditions are supported.



A.11 Time Domain Fiber

The *TimeDomainFiber* is designed to be used with Sample Mode or Aperiodic Block Mode components as it runs with Aperiodic Boundary Conditions. It can be used to model self- and cross- phase modulation, four-wave mixing, stimulated Raman scattering, second- and third-order group velocity dispersion, and frequency-dependent attenuation. A constant state of linear polarization is assumed, as with most components in this tool.

Inputs

leftInput = optical signal input
(signal type: Optical Samples, Optical Blocks)

Outputs

rightOutput = optical signal output
(signal type: Optical Samples, Optical Blocks)

Physical Parameters

Name and Description	Symbol	Unit	Type	Volatile	Value Range	Default Value
Attenuation Attenuation per unit length.	—	dB/m	real	yes]0,10] ^a	0.25e-03
AttenuationSlope Attenuation Slope (w.r.t. wavelength) per unit	—	dB/m ²	real	yes]0,10] ^a	0.0 e+09
AttenuationSecond Deriv Attenuation Second Derivative (w.r.t. wavelength) per unit length	—	dB/m ³	real	yes]0,10] ^a	0.0e+18
Length Fiber Length	—	m	real	yes]0,1000000] ^a	1000
Dispersion Dispersion coefficient.	—	s/m ²	real	yes	[-500.10 ⁻⁶ ,500.10 ⁻⁶] ^w	16e-6
DispersionSlope Slope of the dispersion	—	s/m ³	real	yes	[-10 ³ ,10 ³] ^w	0.08e3
NonLinearIndex Nonlinear index coefficient	—	m ² /W	real	yes	[0,20-10 ²⁰] ^w	2.6e-20
CoreArea Effective core area	—	m ²	real	yes]0,10- ⁷] ^w	80e-12
Tau1 First parameter for Raman response function	—	s	real	yes	[10 ⁻¹⁵ ,50-10 ⁻¹⁵] ^a	12.2e-15
Tau2 Second parameter for Raman response function	—	s	real	yes	[10 ⁻¹⁵ ,50-10 ⁻¹⁵] ^a	32.0e-15
RamanCoefficient Fractional contribution of the delayed Raman response	—	—	real	yes	[0,1] ^a	0.0

Numerical Parameters

Name and Description	Symbol	Unit	Type	Volatile	Value Range	Default Value
Algorithm Algorithm used for dispersion calculation	—	—	enum	no	RECURSIVE, OVERLAPADD	OVERLAPADD
StepSize Step length per dispersion calculation	—	m	real	yes]0,1000000] ^a	1000
MinImpulseLength Minimum Impulse Response Length in overlap add filter.	—		int	no]0,°°] ^a	512

Enhanced Simulation Parameters

Name and Description	Symbol	Unit	Type	Volatile	Value Range	Default Value
SignalType Input signal type.	—	—	enum	no	BLOCKS, SAMPLES	SAMPLES
PhaseFitDump Path of file to dump fitted phase characteristic.	—	—	filename	no	—	—
Tolerance Convergence control parameter for conjugate gradient fitter.	—	—	real	no]0,0.1] ^a	0.001
MaxFilterOrder Maximum filter order per MaxPhaseRange variation.	—	—	int	no]0,°°] ^a	8
MinFilterOrder Maximum filter order per MaxPhaseRange variation.	—	—	int	no]0,°°] ^a	2
StepFilterOrder Maximum filter order per MaxPhaseRange variation.	—	—	int	no]0,°°] ^a	2

Name and Description	Symbol	Unit	Type	Volatile	Value Range	Default Value
MaxRunLength Maximum run length in the conjugate gradient fit.	—	—	int	no]0,100] ^a	5
MaxPhaseRange Maximum phase variation addressed by a single conjugate gradient fitting	—	—	real	no]0,∞] ^a	3.14159
TargetError Target rms phase error.	—	degree	real	no]0,5] ^a	1.0
MaxFrequency Maximum normalized frequency for conjugate gradient fitting.	—	—	real	no	[0,3.14159] ^a	3.14159/2
MinFrequency Minimum normalized frequency for conjugate gradient fitting.	—	—	real	no]−3.14159,0] ^a	−3.14159/2
FrequencyStep Frequency step for conjugate gradient fitting.	—	—	real	yes]0,∞] ^a	0.15

When to Use TimeDomainFiber

The TimeDomainFiber is recommended:

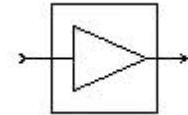
- for linear fiber simulations with aperiodic sources;
- for systems with feedback where the fiber's output influences the behavior of other components;
- (advanced) when fiber computations are the main limitation to an unacceptably slow simulation, and the dispersion conditions allow the computational workload to be reduced by operating in recursive mode. These conditions will usually be only identifiable by experimentation.

The *TimeDomainFiber* is *not* recommended for *quick and dirty* simulations unless you have considerable experience with the *TimeDomainFiber* model. Generally, finding a sensible choice of internal parameters means that simulations involving *TimeDomainFiber* require more patience and work to give sound results than do simulations where another fiber model is applicable.

Do not use *TimeDomainFiber* in recirculating-loops. The *TimeDomainFiber* model maintains its own internal state and thus assumes its input is from a particular physical point in the network. The output is dependent on the input history, which will be distorted and unphysical if it is taken from several different physical network points, as will occur within loops. The same restriction applies to many sample-mode models which have their own internal memories, such as the *LaserTLM* family.

Module Delay

A feature of *TimeDomainFiber* to note is its delay of signals. This is in contrast to the behavior of the module *FiberNLS*, because *FiberNLS* calculates dispersive effects based on a Fourier transform of the entire time window and can thus strip away common-mode delays through the system. Therefore dispersion with zero slope will be calculated by *FiberNLS* to have a zero delay (input and output pulses thus centered at the same position). Because *FiberNLS* addresses the whole time window in one step, it can implement this non-causal behavior to keep all the pulses centered at the same place. In contrast, *TimeDomainFiber* uses time domain filters, which are necessarily causal and hence it can never completely strip away the common-mode pulse delay as *FiberNLS* can [20].



4.12 Ideal Amplifier with Wavelength Independent Gain

This module simulates a system-oriented amplifier with a wavelength-independent gain and noise figure. By parameter selection the module may act in a gain-controlled, output power-controlled, or saturating (uncontrolled) mode. The model is not only restricted to high gain amplifiers but is also valid for low gain and even attenuating amplifiers.

Inputs

input = optical signal
(signal type: *Optical Blocks*, *Optical Samples*)

Outputs

output = optical signal
(signal type: *Optical Blocks*, *Optical Samples*)

Physical Parameters

Name and Description	Symbol	Unit	Type	Volatile	Value Range	Default Value
SystemModelType Selects if the amplifier is internally GAIN-controlled, POWER-controlled or runs into SATURATION.	—	—	enum	yes	Gain, Power, Saturation	Gain
LockedTarget Target (GAIN or POWER) of the amplifier if locked by an internal control-loop	G , P_{out}	dB, dBm	real	yes]-100,100[10
UnsaturatedGain Unsaturated gain of the amplifier. (Only used in SATURATION mode)	G_u	dB	real	yes] $10\log(2)$, ∞ [10

Name and Description	Symbol	Unit	Type	Volatile	Value Range	Default Value
SaturationPower Saturation power at 3-dB-optical-gain-compression. (Only used in SATURATION mode.)	P_{sat}	W	real	yes]0,∞[10.0e-3
SaturationMode Selects where the SaturationPower refers to. (Only used in SATURATION mode.)	___	___	enum	yes	Input, Output	Input
IncludeNoise Selects if the amplifier produces noise.	___	___	enum	yes	On,Off	On
NoiseFigure Noise Figure of the amplifier.	NF	dB	real	yes	[0, ∞[4.0
NoiseBandwidth Total bandwidth over which noise is considered.	___	Hz	real	yes	[0, ∞[4.0e12
NoiseCenterFrequency Center frequency of the bandwidth in which ASE noise is considered.	___	Hz	real	yes	[0, ∞[193.15e12
PolarizFilter A linear-polarization filter can be placed at the output of the amplifier.	___	___	enum	yes	X, Y, None	X

Enhanced Simulation Parameters

Name and Description	Symbol	Unit	Type	Volatile	Value Range	Default Value
NoiseBinSpacing Spacing of ASE Noise Bins.	___	Hz	real	yes	[10.10 ⁶ ,10.10 ¹²]	100e9
RandomNumberSeed Lookup index to use for noise generation. A value of zero implies an automatic unique seed.	___	___	Int	no	[0,10000]	0
Active Defines if the module is active or not.	___	___	enum	no	ON, OFF	ON

Description

This system-level amplifier module consists of an ideal amplifying unit characterized by a frequency-and wavelength-independent gain G according to

$$\mathbf{E}_{\text{out}} = \begin{pmatrix} E_{\text{in},x} \\ E_{\text{in},y} \end{pmatrix} \cdot \sqrt{G} \quad (\text{A.6})$$

It runs in three different modes referring to the amplification behavior. These modes can be selected by parameter **SystemModelType**:

- In the "GAiN"-controlled mode the pump power is variable and the parameter **LockedTarget** specifies the pure input signal amplification.
- In the "POWER"-controlled mode the pump power is variable and the parameter **LockedTarget** specifies the total output power (including the power of the noise that is generated if **IncludeNoise=On**).
- In the "SATURATION" mode the module represents an uncontrolled amplifier with a constant pump power running into internal saturation.

Signal Representation: Individual Samples

For individual samples only the **SystemModelType** = GAIN is supported. Each sample is amplified by Gain. (Not supported in the product Fiber Amplifier.)

Reinitialization Behavior

Multiple Runs and Restart of Simulation are not available

Multiple Runs:

In the first run, a unique seed is occupied by each module if the start seed value was chosen to zero. On consecutive runs, the individual random sequence of each module using the noise generator is continued.

Restart of Simulation:

If the simulation is restarted again, the same seed values from the lookup table are used for noise generation. Note that topology changes may change the specific seed value used by a module.

Module Deactivation:

If **Active** is OFF, the input signal is passed through to the output without any changes.

Comments

The Noise Figure is allowed to fall below NF_{min} , but an instructive warning is thrown.